U.PORTO
FEUP FACULDADE DE ENGENHARIA
UNIVERSIDADE DO PORTO

Master in Mechanical Engineering
Faculty of Engineering of University of Porto
Technische Universität München

Optimization of Reduced Reaction Mechanisms for CFD Simulations of Methane/Hydrogen Flames Under Modern Gas Turbine Conditions

Author:
José Pedro dos Santos Peixoto

Advisor at FEUP:
Abel Rouboa, Ph. D.

Advisor at TUM:
Philip Bonnaire M. Sc.

October 21, 2022

Porto

Acknowledgements

The elaboration of a dissertation thesis is, all things considered, the culmination of years of blood, sweat and tears. It is a brief description of a long journey, a quest where, fortunately, I had the honor of meeting so many amazing people, from all around the world, whom, alas, I may not be able to explicitly mention hereby, but, regardless, I do feel the need to express my sincere gratitude towards.

Alongside friends, both professors and fellow colleagues equally managed help me grow as a person. In that sense I would like to thank both Alex Garcia and Benedikt Biller for all their contribution throughout the makings of this thesis: your expertise accelerated my empirical knowledge on this field and, without your assistance, I am sure I would have struggled much more to conclude this work. Moreover, I would like to also thank Prof. Catarina Castro for your everlasting sense of aiding others. Your kindness and availability, expressed in the form of wise advice, tremendously helped me to ultimately reach my goals. Additionally, I would like to acknowledge Prof. Abel Rouboa for allowing me to pursue my dream of studying abroad.

Furthermore, I would like to express a special thanks to Philip Bonnaire. Combined with a huge knowledge on the field, your leadership skills and big heart made me realize why TUM has managed to become such a prestigious university. Your unparalleled guidance evidently carved this thesis and words cannot describe how much I appreciate it.

Moreover, I would like to thank my sister Inês, my cousins Luis Miguel and Tiago, my uncle Luis Firmino and aunt Mónica Santos for your support throughout my study cycle. I know how proud you all are of this accomplishment and it is as mine as it is yours.

Last, but not least, I would like to give a very special thanks to my parents, Goretti and António, for whom I owe everything, including my name. Your unconditional love and support continuously pushed to me evolve into where I stand today. Your efforts to help me achieve my dreams will never be forgotten and, therefore, from the bottom of my heart, I humbly thank you.

"It's not how you start that's important, but how you finish." - Jim George

Abstract

Modern gas turbines are designed to operate with turbulent reacting flows. This domain is characterized by mutually interacting fluid, chemical and transport phenomena across a broad range of spatial and temporal scales. These interactions are computationally expensive to program, as turbulent-chemistry systems involve, typically, hundreds of elementary reactions and species when modelling. A widely regarded, and preferable, option is to deploy so-called simplified reaction mechanisms, which describe the same overall reaction process, though considering a much smaller amount of reactions and species, whilst providing results with significant accuracy. Also, parameters such as heat release and the addition of hydrogen to the premix promote thermoinstabilities, potentially damaging the burner overtime. Therefore, a deep understanding of flame behaviour is necessary in order to properly model combustion codes.

With that said, the purpose of the present thesis is to investigate the potential use of simplified reaction mechanisms for CFD simulations of premixed air-hydrogen-methane flames under a small scale burner. After an introductory literature review on the effects of turbulence on the flame and vice-versa, it follows afterwards a brief description of a modeled small-scale burner, wherein CFD is performed. Within the scope of flame structure, extracted data, primarily based around heat release and temperature profile analysis, is due across all presented cases.

All in all, the core objective may be reduced into finding an answer to the following questions:

1. in what way does hydrogen influence the flame structure?
2. what is the main difference concerning the usage of FGM vs Complex Chemistry?
3. what are the notable differences observed between using the detailed and reduced mechanisms, respectively?

A premixed air-methane-hydrogen lean flame is displayed, whose shape does not corroborate the current literature review and, therefore, an observation is due. Also, temperature profiles are provided, wherein flame shape structure may be viewed according to the corresponding cases' closure models. Furthermore, results show a similar behaviour between the reduced and detailed mechanisms, namely in the indicated mean chemistry heat release rate profiles and geometric center of flame relative coordinates, which corroborates the possibility and potential of applying reduced mechanisms in future combustion codes of lean-premixed mixtures of air-hydrogen-methane in modern combustion systems.

Resumo

Atualmente, as turbinas a gás são dimensionadas para operar sob regime de combustão turbulenta, que é caracterizado por uma interação mútua e simultânea entre as diversas espécies que constituem o fluido circulante, acarretando ainda fenómenos químicos e de transporte, que ocorrem ao longo de um vasto conjunto de escalas de tempo e espaço. Trata-se de um processo computacional dispendioso, na medida em que requere a modelização de centenas de espécies, intervenientes em milhares de reações. Uma alternativa unanimemente aceite acenta na implementação de mecanismos simplificados, que contêm apenas os elementos e respetivas reações mais preponderantes do processo de combustão, reduzindo assim o custo, enquanto mantém uma proximidade de resultados face ao verificado em mecanismos mais detalhados. Paralelamente, parâmetros como transferência de calor e teor de hidrogénio invocam instabilidades que danificam a longo prazo a câmara de combustão. Tudo isto requer um profundo conhecimento sobre comportamento de chama.

Assim, a presente tese propõe investigar o potencial uso de mecanismos simplificados em CFD de chamas com pré-mistura de ar-hidrogénio-metano num combustor recriado de pequena escala. Após uma breve introdução teórica dos efeitos de turbulência em chamas e vice-versa, segue-se uma rápida descrição do design e configuração adotados, bem como uma análise estrutural da chama, tendo por base o estudo de perfis de temperatura e transferência de calor.

Em suma, o trabalho proposto traduz-se na procura por uma resposta às seguintes perguntas:

1. de que modo o hidrogénio influencia a estrutura da chama?
2. quais as principais diferenças na utilização de FGM vs Complex Chemistry?
3. quais as diferenças observadas entre o uso de mecanismos simplificados comparativamente com mecanismos detalhados?

O primeiro caso exposto onde é adicionado hidrogénio apresenta características contraditórias face ao encontrado na literatura, sendo feita uma observação nesse sentido. Além disso, são apresentados perfis de temperatura onde é possível observar a performance dos diversos modelos testados. Quanto à análise do comportamento demonstrado pelos mecanismos, constatam-se semelhanças a nível de transferência de calor e centro geométrico de chama, que corroboram a possibilidade de se explorar a utilização de mecanismos simplificados em programação de chama com pré-mistura de air-hidrogénio-metano em modelos modernos de combustão.

Contents

List of Figures **12**

List of Tables **13**

Nomenclature **15**

1 Introduction **17**

2 Theory **19**
2.1 Reacting flows . . . 19
2.1.1 Momentum equation . . . 19
2.1.2 Mass and species equation . . . 19
2.1.3 Energy equation . . . 20
2.2 Laminar premixed flames . . . 21
2.2.1 Governing equations . . . 21
2.2.2 Input influence . . . 22
2.2.3 Theoretical solutions . . . 22
2.3 Turbulent premixed flames . . . 25
2.3.1 Introduction . . . 25
2.3.2 CFD . . . 25
2.3.3 RANS . . . 26
2.3.4 LES . . . 27
2.4 Chemistry for turbulent combustion . . . 31
2.4.1 Introduction . . . 31
2.4.2 Reduced chemical models . . . 31
2.4.3 Chemistry closure models . . . 32
2.4.4 Turbulence-chemistry closure models: TFC . . . 36

3 Burner configuration **39**
3.1 Introduction . . . 39
3.2 Geometry . . . 39
3.3 Operating conditions . . . 39
3.4 Numerical details . . . 41
3.5 Model description . . . 43
3.6 Initializing solver . . . 45

4 Results **47**
4.1 Introduction 47
4.2 Addition of hydrogen to the premixed fuel 48
4.3 RANS vs LES 49
4.4 FGM vs Complex Chemistry 49
4.5 Detailed vs Reduced mechanisms 51

5 Conclusions **57**

6 Future accomplishments **59**

Appendices **61**

A Chapter 2 **63**
A.1 Averaging the balance equations: RANS 63

Bibliography **65**

List of Figures

2.1 Input parameter study of s_L (taken from Aung et.al.[1]). 23
2.2 DNS-RANS-LES performance on computing time vs local temperature in turbulent flame brush (taken from Staffelback[46]). 26
2.3 RANS vs LES temperature profile representation and comparison across a swirled combustor with turbulent combustion[41]. 27
2.4 Velocity data in turbulent premixed flame[50]. Velocity probabilities are displayed in location: (a): fresh gases; (b): mean reaction zone; (c): burnt gases. 28
2.5 Simplified illustration of (from left to right): a turbulent flow containing differently sized eddies; overview of grid and sub-grid scale turbulent eddies[5, 31]. 28
2.6 Gaussian filter[36]. 29
2.7 Illustration of a flamelet[43]. 33
2.8 Cross-section of progress variable profile (reduced temperature in this case) for STAR-CCM+. The variable ranges from 0 (fresh gas) and 1.0 (burnt gas). 35
2.9 Illustration of reacting species transport[43]. 36

3.1 Side view of the geometry used in numerical study with flow moving from right to left: 1) Exhaust distribution duct; 2) Combustion chamber; 3) Premixing duct; 4) Entrance to converging-diverging nozzle. 40
3.2 Front view of the combustion chamber. 40
3.3 Cross-section view of the CFD mesh: 1) Combustion chamber; 2) Flame region; 3) Premixing duct; 4) Exhaust gas distribution duct. 42
3.4 Cross-section view of the cell length across the burner. 42
3.5 Cross-section view of the CFL number across the burner. 43

4.1 Mean of chemistry heat release rate for case I. 48
4.2 Mean of chemistry heat release rate for case II. 48
4.3 Instantaneous temperature profile of case II. 49
4.4 Instantaneous temperature profile of case III. 50
4.5 Instantaneous temperature profile of case IV. 50
4.6 Mean of chemistry heat release rate for case IV. 51
4.7 Instantaneous temperature profile of case V. 52
4.8 Mean of chemistry heat release rate profile for case V. 52
4.9 Evolution of the relative coordinates of the geometric center of flame for case I. 53
4.10 Evolution of the relative coordinates of the geometric center of flame for case II. 54
4.11 Evolution of the relative coordinates of the geometric center of flame for case III. 54
4.12 Evolution of the relative coordinates of the geometric center of flame for case IV. 55
4.13 Evolution of the relative coordinates of the geometric center of flame for case V. 55

List of Tables

2.1 Turbulent closure model overview[36]. 25

3.1 Operating conditions for all tested cases[28]. 41
3.2 Details on used CFD mesh. 43
3.3 CFL numbers for relevant regions. 44
3.4 CFD settings for case I. 44
3.5 CFD settings for case II. 44
3.6 CFD settings for case III. 44
3.7 CFD settings for case IV and V. 45

4.1 Description of the major characteristics of each of the four analysed cases. 47
4.2 Relative coordinates of the geometric center of flame for all DLR cases. . . 53

Nomenclature

Roman Symbols

$\dot{\mathcal{Q}}$	Heat source term	[W/m^3]
e_t	Total energy	[J]
f_{kj}	Volume force	[J/(mkg)]
h_t	Total enthalpy	[J/kg]
I_l	Turbulent length scale	[m]
Q^m	Molar heat of reaction	[J/mole]
q_i	Energy flux	[W/m^2]
s_L	Laminar flame speed	[m/s]
$V_{k,i}$	Diffusion velocity	[m^2/s]
Y	Reduced mass fraction	[-]
F	LES filter	[-]
f	Quantity	
G	Stretch factor	[-]

Greek Symbols

α_u	Unburnt thermal diffusivity	[m^2/s]
$\dot{\omega}_F$	Fuel mass fraction reaction rate	[kg/(m^{3}s)]
$\dot{\omega}_{\mathrm{Y}}$	Progress variable source term	[-]
$\dot{\omega}_\Theta$	Reaction rate for reduced temperature Θ	[kg/(m^{3}s)]
$\dot{\omega}_T$	Heat release source term	[kg/(m^{3}s)]

μ	Dynamic viscosity	[Ns/m^2]
ν_L	Laminar burning velocity	[m/s]
ν_T	Turbulent flame speed	[kg/(s^{2}m)]
Φ	Viscous heating source term	[Pa/s]
ρ	Density	[kg/m^3]
τ_{SGS}	Sub-grid stress	[Pa]
Θ	Reduced temperature	[-]

Acronyms

CFD	Computational Fluid Dynamics
DNS	Direct Numerical Simulation
EBU	Eddy Break-Up
EDC	Eddy Dissipation Concept
FGM	Flamelet Generated Manifold
ISAT	In-Situ Adaptive Tabulation
LFC	Laminar Flame Concept
PDF	Probability Density Function
PPDF	Presumed Probability Density Function
RANS	Reynolds Averaged Navier Stokes
SGS	Sub-grid scale
TFM	Thickened Flame Model
WALE	Wall-Adapting Local Eddy-Viscosity

1 Introduction

Combustion can be reduced to the oxidation of fuel[25]. Even thought this definition proves to be objective and simple to understand, the process itself can be rather complex, as turbulence and chemical effects have to be simultaneously accounted in (un)steady flows. In more recent modern gas turbine installations, operating settings have been implemented with the goal to minimize NO_x emissions bellow 10 ppm[18].

In that regard, turbulent combustion involves non-linear multi-scale interactions between molecular, transport and fluid motions that shape flame and flow behaviour[47]. To model the resulting flames from the combustion process, a lot of knowledge on the field is mandatory: a plethora of parameters, such as the equivalence ratio, mass fraction, mass flow, heat release, flame speed, concentration of hydrogen in the (premixed) flame, among others, affect the overall flame behaviour[55], which means it is important to know beforehand in what way these properties influence the flame structure[7]. Alongside, a deep understanding of the turbulence, chemistry and turbulence-chemistry closure models proves to be critical in order to develop and improve practical systems[36].

Both turbulence and chemistry closure models carry a lot of computational cost, specially when modeling such complex regimes[39]. The latter model increases exponentially in difficulty, as the number of reactions is normally thrice the amount of invoked species, which are of the order of the hundreds[36]. The current alternative lies on the implementation of detailed mechanisms, but, such mechanisms still contain a considerable amount of species and reactions, thus, it is currently considered as a costly option[37]. The new approach is to find reduced mechanisms, i.e., chemical schemes that contain only the predominant chemical equations that determine the chemical scheme, thereby reducing in a significant way the amount of time necessary to conduct CFD[32].

With that said, the present work aims to investigate the potential use of reduced mechanisms in turbulent combustion flows, by analysing the flame structure in accordance to the type of models used, mainly focusing on two specific parameters: heat release and the addition of hydrogen to the premix, respectively.

2 Theory

2.1 Reacting flows

Gas Turbines are characterized by operating under continuous reacting flows. For such regime, a reacting gas[i] is burned in order to extract useful thermal energy, which, afterwards, can be converted either into mechanical or electrical energy.

With that said, this chapter will focus on the numerical implications of flame coding. The derivation of the conservation equations for reacting flows, obtained from the mass, species and energy balances in the upcoming sections might be found in the works of Poinsot et.al.[36], and furthermore in Williams[52], Kuo[21] or Candel[3].

2.1.1 Momentum equation

Starting with the momentum equation, for both reacting and non-reacting flows, it can be written the same way[36]:

$$\frac{\partial}{\partial t}\rho u_j + \frac{\partial}{\partial x_i}\rho u_i u_j = -\frac{\partial p}{\partial x_j} + \frac{\partial \tau_{ij}}{\partial x_i} + \rho \sum_{k=1}^{N} Y_k f_{kj} = \frac{\partial \sigma_{ij}}{\partial x_i} + \rho \sum_{k=1}^{N} Y_k f_{kj} \tag{2.1}$$

where f_{kj} is the volume force of species k applied in direction j. Although this equation does not include explicit reaction terms, parameters such as the dynamic viscosity, μ, density, ρ, and the dilation through the flame front change due to combustion effects[2]. This leads to a more significant increase of the local Reynolds number, compared to the non-reactive counterpart[39], which means that, despite sharing the same equation, the observed flow behaviour for both regimes might be rather different[36].

2.1.2 Mass and species equation

Similarly to the prior governing formula, the equation for the conservation of mass remains unchanged for both reacting and non-reacting cases[36]:

$$\frac{\partial \rho}{\partial t} + \frac{\partial \rho u_i}{\partial x_i} = 0 \tag{2.2}$$

[i] Non-isothermal mixture of multiple species such as, for example, hydrocarbons, oxygen, water or carbon dioxide, amongst others, which must be tracked individually[36].

since combustion does not generate new mass, ergo, the mass conservation equation may be written like[36]:

$$\frac{\partial \rho Y_k}{\partial t} + \frac{\partial}{\partial x_i}\left(\rho Y_k \left(u_i + V_{k,i}\right)\right) = \dot{\omega_k} \tag{2.3}$$

where $\dot{\omega_k}$ is the reaction rate and $V_{k,i}$ the diffusion velocity of the i-th component. Both are as follows[36]:

$$\sum_{k=1}^{N} Y_k V_{k,i} = 0 \quad \text{and} \quad \sum_{k=1}^{N} \dot{\omega_k} = 0 \tag{2.4}$$

2.1.3 Energy equation

The following section deduces the energy terms while showing a reason (of many) on why it is hard to artificially configure flames.

Due to the continuity equation (Eq. (2.2)), any quantity f may be[36]:

$$\rho \frac{Df}{Dt} = \rho\left(\frac{\partial f}{\partial t} + u_i \frac{\partial f}{\partial x_i}\right) = \frac{\partial \rho f}{\partial t} + \frac{\partial \rho u_i f}{\partial x_i} \tag{2.5}$$

Using as input the total energy, e_t[21, 36]:

$$\rho \frac{De_t}{Dt} = \frac{\partial \rho e_t}{\partial t} + \frac{\partial}{\partial x_i}\left(\rho u_i e_t\right) = -\frac{\partial q_i}{\partial x_i} + \frac{\partial}{\partial x_j}\left(\sigma_{ij} u_i\right) + \dot{\mathcal{Q}} + \rho \sum_{k=1}^{N} Y_k f_{k,i}\left(u_i + V_{k,i}\right) \tag{2.6}$$

wherein the heat source is indicated by $\dot{\mathcal{Q}}$. Subsequently, the energy flux, q_i, may be derived[36]:

$$q_i = -\lambda \frac{\partial T}{\partial x_i} + \rho \sum_{k=1}^{N} h_k Y_k V_{k,i} \tag{2.7}$$

Furthermore, combining Eq. (2.2) with enthalpy $h_t = e_t + p/\rho$, and afterwards erasing e_t, establishes[24, 36]:

$$\rho \frac{Dh_t}{Dt} = \frac{\partial \rho h_t}{\partial t} + \frac{\partial}{\partial x_i}\left(\rho u_i h_t\right) = \frac{\partial p}{\partial t} - \frac{\partial q_i}{\partial x_i} + \frac{\partial}{\partial x_j}\left(\tau_{ij} u_i\right) + \dot{\mathcal{Q}} + \rho \sum_{k=1}^{N} Y_k f_{k,i}\left(u_i + V_{k,i}\right) \tag{2.8}$$

The resulting sum of sensible and chemical energy, e, may firstly be reached through the kinetic energy equation, $u_j u_j/2$, and thereafter conducting the product between the momentum equation (Eq. (2.1)), and u_j[36]:

$$\frac{\partial}{\partial t}\left(\frac{1}{2}\rho u_j u_j\right) + \frac{\partial}{\partial x_i}\left(\frac{1}{2} u_i u_j u_j\right) = u_j \frac{\partial \sigma_{ij}}{\partial x_i} + \rho \sum_{k=1}^{N} Y_k f_{k,j} u_j \tag{2.9}$$

only to be subtracted with Eq. (2.6), therefore creating[24]:

$$\rho \frac{De}{Dt} = \frac{\partial \rho e}{\partial t} + \frac{\partial}{\partial x_i}\left(\rho u_i e\right) = -\frac{\partial q_i}{\partial x_i} + \sigma_{ij} \frac{\partial u_i}{\partial x_j} + \dot{\mathcal{Q}} + \rho \sum_{k=1}^{N} Y_k f_{k,i} V_{k,i} \tag{2.10}$$

Similarly, an alternative equation for enthalpy, h, may be equally achieved[24]:

$$\rho\frac{Dh}{Dt} = \frac{\partial\rho h}{\partial t} + \frac{\partial}{\partial x_i}\left(\rho u_i h\right) = \frac{Dp}{Dt} - \frac{\partial q_i}{\partial x_i} + \tau_{ij}\frac{\partial u_i}{\partial x_j} + \dot{\mathcal{Q}} + \rho\sum_{k=1}^{N} Y_k f_{k,i} V_{k,i} \tag{2.11}$$

wherein the viscous heat is amounted by Φ[36]:

$$\Phi = \tau_{ij}\partial u_i/\partial x_j \tag{2.12}$$

Thus, whether from chemical ($\sum_{k=1}^{N}\Delta h^o_{f,k}Y_k$), or transport ($q_i$) nature, the newly obtained equations bring terms, such as $\rho\sum_{k=1}^{N} h_k Y_k V_{k,i}$, whose implementation further difficulties the CFD of flames[36].

2.2 Laminar premixed flames

Beyond being just a more restrictive type of flame, laminar premixed flames may be considered an initial step towards computing turbulent premixed flames[38], as they often serve as the foundation for more intricate structures (see Sec. §2.3). The lesser amount of degrees of freedom allow an evaluation of instabilities[52] in the flame front related to flame thickness, or flame stretch[7], as well as to provide good initial solutions[36].

Nevertheless, even in this simpler regime, other difficulties are imposed, as the next section exemplifies.

2.2.1 Governing equations

Simplified from Sec. §2.1, the following governing equations describe a 1D laminar flame with premix[36]:

- Mass:

$$\frac{\partial\rho}{\partial t} + \frac{\partial\rho u}{\partial x} = 0 \tag{2.13}$$

- Species:

$$\frac{\partial\rho Y_k}{\partial t} + \frac{\partial}{\partial x}\left(\rho\left(u + V_k\right)Y_k\right) = \dot{\omega}_k \tag{2.14}$$

- Energy:

$$\rho C_p\left(\frac{\partial T}{\partial t} + u\frac{\partial T}{\partial x}\right) = \dot{\omega}'_T + \frac{\partial}{\partial x}\left(\lambda\frac{\partial T}{\partial x}\right) - \rho\frac{\partial T}{\partial x}\left(\sum_{k=1}^{N} C_{p,k}Y_k V_k\right) \tag{2.15}$$

  where $\dot{\omega}'_T = -\sum_{k=1}^{N} h_k\dot{\omega}_k$ is an alternate term for the heat release associated with the process of combustion[36].

The aforementioned system can be described with respect to the flame speed, s_L[36]:

$$\rho u \quad = \quad \text{constant} \quad = \quad \rho_1 s_L \tag{2.16}$$

$$\frac{\partial}{\partial x}\left(\rho\left(u+V_k\right)Y_k\right) = \dot{\omega}_k \tag{2.17}$$

$$\rho C_p u \frac{\partial T}{\partial x} = \dot{\omega}'_T + \frac{\partial}{\partial x}\left(\lambda \frac{\partial T}{\partial x}\right) - \rho \frac{\partial T}{\partial x}\left(\sum_{k=1}^{N} C_{p,k} Y_k V_k\right) \tag{2.18}$$

Solving this group of equations remains a task since the reaction rate term, $\dot{\omega}_k$, needs to be closed[36]. To do so, a possible option is recurring to the Arrhenius law[12], in conjunction with established boundary conditions[50], whilst knowing the diffusion velocities[52].

2.2.2 Input influence

Investigating the specific effect of each input parameter has been established as a needed phase to comprehend which variables dominate a given flame quantity[23, 36].

In order to avoid re-running a code to consult results, for instance, one could differentiate the whole code by utilizing sensitivity analysis tools[10, 26], further acquiring a better understanding of the impact of each parameter[1, 9, 14]. For instance, Fig. 2.1 showcases a sensitivity analysis of flame speeds for a certain type of flame in vacuum (0.35 atm) and room temperature conditions[1]. Four values for ϕ were studied (between 0.45 and 3.5). Results revealed the following equation: $OH + H_2 \Leftrightarrow H + H_2O$ is the fundamental aspect to determine the flame speed, which means an optimal way to solve such variable would be to focus strictly on this reaction[36].

2.2.3 Theoretical solutions

Further tackling other issues associated with turbulent combustion demands taking a look at different configurations (beyond the already mentioned one-dimensional planar steady premixed flame) must be studied and understood. To do so, simplifications of chemistry and transport, at a fluid mechanics level, must be made[36]. With that said, the present section goes in-depth about some analytical results that hold extremely impactful implications for numerical combustion[38].

Conservation equations for one-step chemical schemes

In order to reach the conservation equations for this model, a set of simplifications is hereby listed[52]:

- an equal value for the molecular weight, heat capacity and molecular diffusion coefficient is attributed to all species[36],

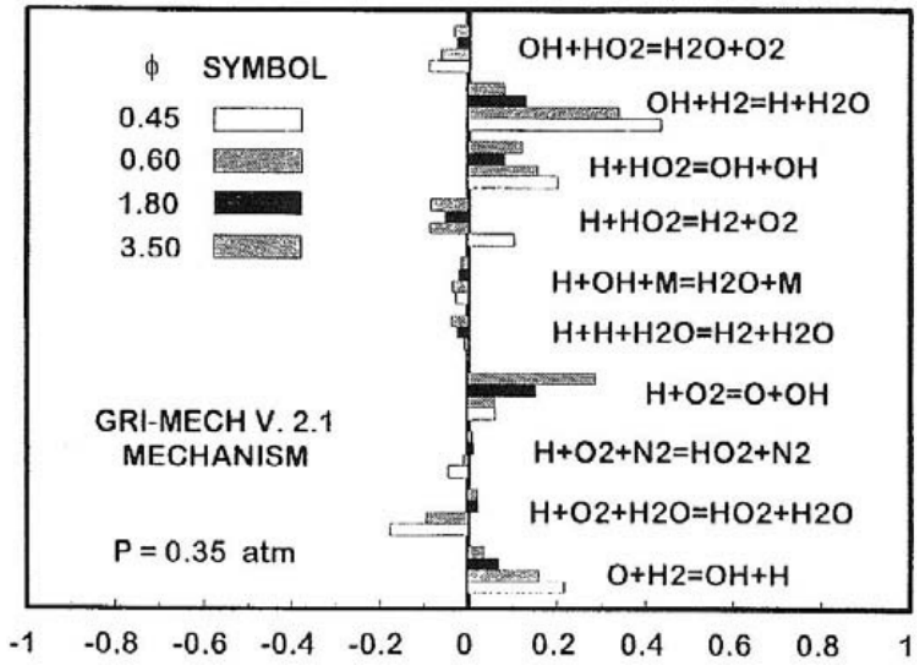


Figure 2.1: Input parameter study of s_L (taken from Aung et.al.[1]).

- chemistry proceeds only through one irreversible reaction[52]:

$$\sum_{k=1}^{N} \nu'_{k1}\mathcal{M} \rightarrow \sum_{k=1}^{N} \nu''_{k1}\mathcal{M} \tag{2.19}$$

which forces the reverse reaction rate to be null. The temperature dependence of the forward reaction allows the establishment of a relation with the Arrhenius law[12]: $K_{f1} = A_1 T^{\beta_1} e^{-T_{a1}/T}$. Furthermore, the following relation is also admitted[36]:

$$\frac{\dot{\omega}_k}{W_k \nu_{k1}} = \mathcal{Q}_1 \quad \text{or} \quad \dot{\omega}_k = W_k \nu_{k1} \mathcal{Q}_1 \tag{2.20}$$

henceforth[36]:

$$\dot{\omega}_T = -\sum_{k=1}^{N} \Delta h^o_{f,k} \dot{\omega}_k = -\mathcal{Q}_1 \sum_{k=1}^{N} \left(\Delta h^o_{f,k} W_k \nu_{k1}\right) = |\nu_{F1}|\, Q^m \mathcal{Q}_1 \tag{2.21}$$

with the molar component of the heat of reaction being given by Q^m[36]:

$$Q^m = -\sum_{k=1}^{N} \Delta h^o_{f,k} W_k \frac{\nu_{k1}}{|\nu_{F1}|} = -\sum_{k=1}^{N} \Delta h^{o,m}_{f,k} \frac{\nu_{k1}}{|\nu_{F1}|} = \sum_{k=1}^{N} \Delta h^{o,m}_{f,k} \frac{\nu_{k1}}{\nu_{F1}} \tag{2.22}$$

- $\dot{\omega}_F$, of reaction described in Eq. (2.19), is presumed as function of the fuel mass fraction[36]. Such assumption translates into studying a state wherein $Y_O = Y_O^1$, meaning Y_F becomes exclusively dependant on the reaction rate[36].

Respecting the aforementioned restrictions, and imposing the fuel mass fraction, Y_F, yields[36]:

$$\rho u = \text{constant} = \rho_1 u_1 = \rho_1 s_L \tag{2.23}$$

$$\rho_1 s_L \frac{dY_F}{dx} = \frac{d}{dx}\left(\rho D \frac{dY_F}{dx}\right) + \dot{\omega}_F \tag{2.24}$$

$$\rho_1 C_p s_L \frac{dT}{dx} = \frac{d}{dx}\left(\lambda \frac{dT}{dx}\right) - Q\dot{\omega}_F \tag{2.25}$$

Reduced fuel mass fraction and temperature

Introducing the following dimensionless variables simplifies Eqs. (2.24) and (2.25)[36]:

$$Y = Y_F/Y_F^1 \quad \text{and} \quad \Theta = \frac{C_p\left(T - T_1\right)}{QY_F^1} = \frac{T - T_1}{T_2 - T_1} \tag{2.26}$$

Combining Eqs. (2.24) and (2.25) provides with[36]:

$$\rho_1 s_L \frac{dY}{dx} = \frac{d}{dx}\left(\rho D \frac{dY}{dx}\right) + \dot{\omega}_F/Y_F^1 \tag{2.27}$$

$$\rho_1 s_L \frac{d\Theta}{dx} = \frac{d}{dx}\left(\frac{\lambda}{C_p}\frac{d\Theta}{dx}\right) - \dot{\omega}_F/Y_F^1 \tag{2.28}$$

Summing the above equations whilst assuming unity Lewis number produces[36]:

$$\rho_1 s_L \frac{d}{dx}\left(\Theta + Y\right) = \frac{d}{dx}\left[\rho D \frac{d}{dx}\left(\Theta + Y\right)\right] \tag{2.29}$$

If Y moves from 1 to 0, Θ will go the other way around, which means the only solution to Eq. (2.29) is the following identity[43]:

$$\Theta + Y = 1 \tag{2.30}$$

From a numerical perspective, due to their inherent dependence, Θ needs to be determined (whereas Y is obtained via Eq. (2.30)). This means an additional equation to calculate the reduced temperature is required[52], that being:

$$\begin{aligned} \rho_1 s_L \frac{d\Theta}{dx} =& \frac{d}{dx}\left(\frac{\lambda}{C_p}\frac{d\Theta}{dx}\right) \\ -B_1\left(T_1 + \Theta\left(T_2 - T_1\right)\right)^{\beta_1} \rho\left(1 - \Theta\right) \exp&\left(-\frac{T_{a1}}{T_1 + \Theta\left(T_2 - T_1\right)}\right) \end{aligned} \tag{2.31}$$

Table 2.1: Turbulent closure model overview[36].

Approach	Advantages	Drawbacks
RANS	- "coarse" numerical grid - geometrical simplification (2D flows, symmetry,...) - "reduced" numerical costs	- only mean flow field - models required
LES	- contains unsteady submodels - "smoother" flow view	- models required - 3D simulations required - computational cost

2.3 Turbulent premixed flames

2.3.1 Introduction

Turbulent combustion essentially represents a flow that combines turbulence and chemistry effects[43]. Numerical combustion has emerged as a viable tool to fill in the obstacles imposed by turbulent flows, namely[52]:

- the fact that combustion itself involves a vast array of differently sized scales[39],
- the fact that turbulence itself equally demands various time and length scales when solving the unclosed terms[36],
- the interplay between chemistry effects and turbulence phenomena, resulting, for instance, in "flame-generated turbulence"[36], or flame quenching[4].

In order to deal with these aspects, the following sections will discuss the mainly used closure models.

2.3.2 CFD

At the present time, one of the most used tools concerning the study of turbulence and combustion effects is a technology commonly denoted as Computational Fluid Dynamics or CFD[17]. This tool allows for the numerical solving of system governing equations, so that the flow of fluids in complex geometries may be visualized[7].

Several methods are being created to solve Navier-Stokes equations[38]. Each method varies in terms of computational effort as well as in scale of obtained accuracy[52]. A general tier list, from the least to most computational intensive could be made[36]: RANS, Unsteady-Reynolds-Averaged Navier-Stokes (URANS), LES and lastly Direct Numerical Simulation (DNS). Table 2.1 highlights the main aspects of the utilized turbulence closure models (RANS and LES respectively).

The fact that both RANS and URANS optimally determine temperature distributions makes them popular solvers[36], however, for the purpose of this work, LES shines by being capable of capturing all the main effects of thermoinstabilities[7, 22, 43], providing with a fairly good accuracy the mean chemistry heat release, a key parameter in flame structure analysis[37].

2.3.3 RANS

Reynolds-Averaged Navier Stokes (RANS) set the foundations of CFD. Fundamentally, it averages the instantaneous governing equations[36, 52]. Subsequently, the newly extracted mean quantities demand closure rules[43]. Moreover, Fig. 2.2 shows an example of application of RANS for a stabilized flame[46], where the predicted temperature is equal to the mean temperature at a certain point[36].

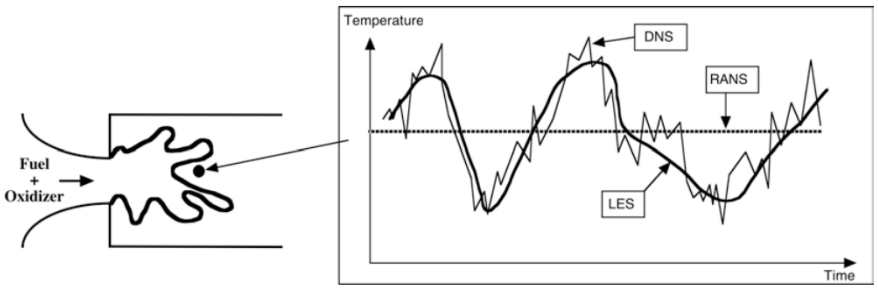


Figure 2.2: DNS-RANS-LES performance on computing time vs local temperature in turbulent flame brush (taken from Staffelback[46]).

Averaged balance equations for one-step premixed turbulent flame

As suggested in Sec. §2.2.3, consider the following reaction[36]:

$$R \quad \text{(reactants)} \quad \rightarrow \quad P \quad \text{(products)} \tag{2.32}$$

Generally, combustion codes for turbulent premixed flames carry the assumption of unity Lewis numbers, constant pressure and adiabatic conditions[36]. Under such restrictions, the relation linking the reduced temperature Θ, to the reduced reactant mass fraction, Y, still remains valid ($\Theta = \frac{C_p(T-T_1)}{QY_F^1}$)[36]. Ergo, and as explained previously, only one of the above parameters shall need to be retained.

Thereafter, the system describing turbulent low-speed premixed flame is[36]:

$$\frac{\partial \overline{\rho}}{\partial t} + \frac{\partial}{\partial x_i}\left(\overline{\rho}\tilde{u}_i\right) = 0 \tag{2.33}$$

$$\frac{\partial \overline{\rho}\tilde{u}_j}{\partial t} + \frac{\partial}{\partial x_i}\left(\overline{\rho}\tilde{u}_i\tilde{u}_j\right) + \frac{\partial \overline{p}}{\partial x_j} = \frac{\partial}{\partial x_j}\left(\overline{\tau}_{ij} - \overline{\rho}\widetilde{u_i'' u_j''}\right) \tag{2.34}$$

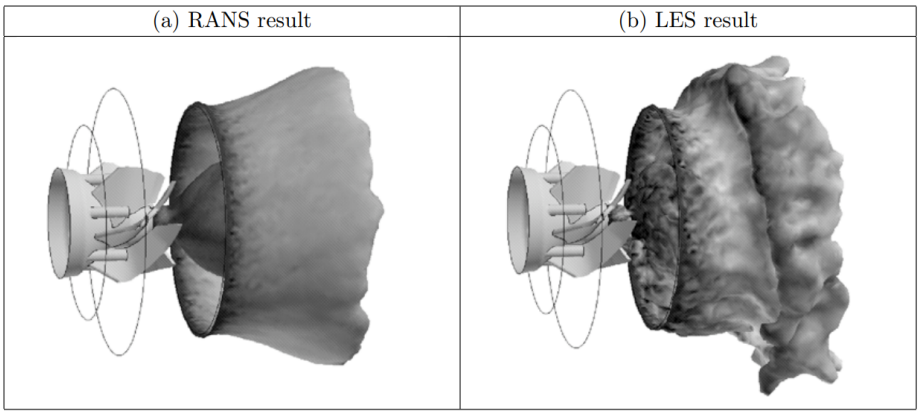


Figure 2.3: RANS vs LES temperature profile representation and comparison across a swirled combustor with turbulent combustion[41].

$$\frac{\partial\left(\overline{\rho}\tilde{\Theta}\right)}{\partial t}+\frac{\partial}{\partial x_i}\left(\overline{\rho}\tilde{u}_i\tilde{\Theta}\right)=\frac{\partial}{\partial x_i}\left(\overline{\rho}\overline{D}\frac{\partial\tilde{\Theta}}{\partial x_i}-\overline{\rho}\widetilde{u_i''\Theta''}\right)+\overline{\dot{\omega}}_\Theta \tag{2.35}$$

Because only $\overline{\rho}$, $\tilde{u}_i$ and $\tilde{\Theta}$ are unknowns, the initial set of averaged equations can be simplified even further, yet, one still has to be careful with the following consequent unclosed terms which require modeling[36]:

- the turbulent stress tensor, $\overline{\rho u_i'' u_j''}$,
- the mean reduced temperature reaction rate, $\overline{\dot{\omega}}_\Theta$,
- the transport parameter $\overline{\rho u_i''\Theta''}$.

2.3.4 LES

Large eddy simulations (LES) purpose is, ultimately, to compute, in an explicit way, the largest structures of flow field, modeling the small sized ones[36]. Such approach can be quite useful, specially because, seldom, it is not necessary to resolve all the turbulent scales in a flow[36], as only looking at the larger directionally dependent scales, whilst modeling the mostly universal smaller ones, grid sizes, as well as time steps, may be increased to reduce computational cost[38]. The way the filtering process functions will be further explained in the upcoming section.

The instantaneous governing equations suffer a filtering process[52]. A practical application of LES would be therein Fig. 2.2, where a low-frequency spectrum of temperature is captured[46].

LES filters

A concerning issue in LES of premixed flames is the fact the its mesh size is typically larger than the flame thickness, δ_L^0[51]. Consequently, computing the progress variable will likely

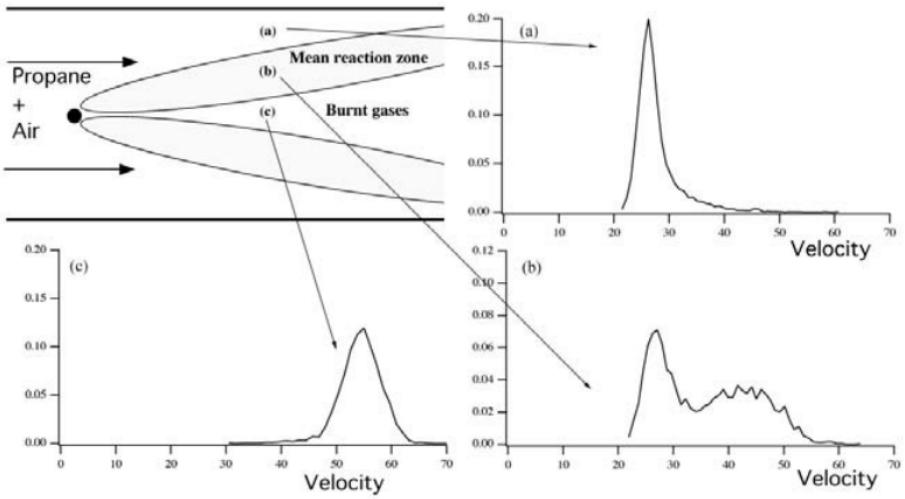


Figure 2.4: Velocity data in turbulent premixed flame[50]. Velocity probabilities are displayed in location: (a): fresh gases; (b): mean reaction zone; (c): burnt gases.

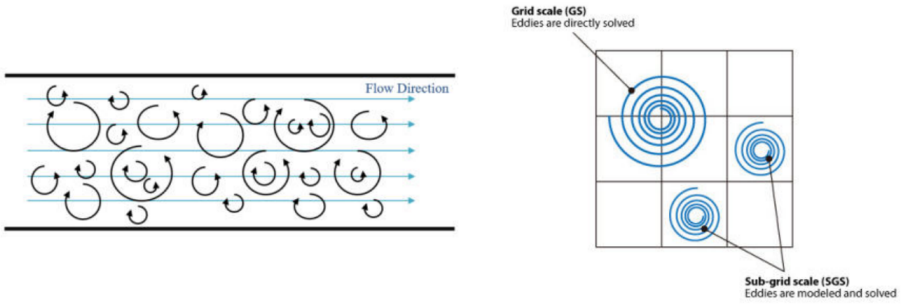


Figure 2.5: Simplified illustration of (from left to right): a turbulent flow containing differently sized eddies; overview of grid and sub-grid scale turbulent eddies[5, 31].

bring problems[36]. The present section will therefore discuss the proposed alternative, which is the gaussian filter.

Structures smaller than the grid size are typically referred to as sub-grid scale, while the larger ones are called the grid or resolved scales[39]. Fig. 2.5 illustrates the aforementioned notions. The averaged quantities are numerically solved while its fluctuations are filtered due to the fact that they are smaller than the sub-grid scales[19]. Plenty of filter functions are available on LES[36] but, in the end, it all comes down to the same principle: dividing the structures into the resolved and sub-grid scale components[39].

Gaussian filter parameters result of either a suppression of values larger than a given quantity, or, from performing a weighted average for a certain quantity[36]. A representation of this filtering operation can be observed in Fig. 2.6.

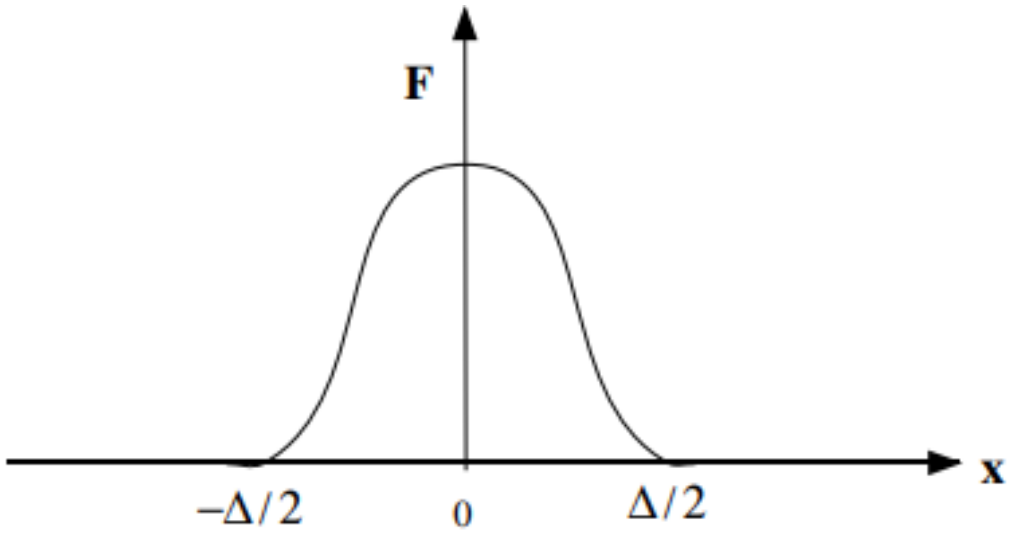


Figure 2.6: Gaussian filter[36].

For a filter F, the gaussian filter may be mathematically expressed as follows[36]:

$$F(\mathbf{x}) = F(x_1, x_2, x_3) = \left(\frac{6}{\pi\Delta^2}\right)^{3/2} \exp\left[-\frac{6}{\Delta^2}(x_1^2 + x_2^2 + x_3^2)\right] \tag{2.36}$$

Governing equations post filtering

Similarly to the system derived in Sec. §A.1, the governing equations post filtering are as follows[36]:

- Mass:

$$\frac{\partial\overline{\rho}}{\partial t} + \frac{\partial}{\partial x_i}(\overline{\rho}\tilde{u}_i) = 0 \tag{2.37}$$

- Momentum:

$$\frac{\partial\overline{\rho}\tilde{u}_i}{\partial t} + \frac{\partial}{\partial x_i}(\overline{\rho}\tilde{u}_i\tilde{u}_j) + \frac{\partial\overline{p}}{\partial x_j} = \frac{\partial}{\partial x_j}\left[\overline{\tau}_{ij} - \overline{\rho}\left(\widetilde{u_i u_j} - \tilde{u}_i\tilde{u}_j\right)\right] \tag{2.38}$$

- Chemical species:

$$\begin{aligned}\frac{\partial\left(\overline{\rho}\tilde{Y}_k\right)}{\partial t} + \frac{\partial}{\partial x_i}\left(\overline{\rho}\tilde{u}_i\tilde{Y}_k\right) = \frac{\partial}{\partial x_i}\left[\overline{V_{k,i}Y_k} - \overline{\rho}(\widetilde{u_i Y_k} - \tilde{u}_i\tilde{Y}_k)\right] \\ + \overline{\dot{\omega}}_k \quad \text{for} \quad k = 1, N\end{aligned} \tag{2.39}$$

- Enthalpy:

$$\begin{aligned}\frac{\partial \overline{\rho}\tilde{h}_s}{\partial t} + \frac{\partial}{\partial x_i}\left(\overline{\rho}\tilde{u}_i\tilde{h}_s\right) = \overline{\frac{Dp}{Dt}} + \frac{\partial}{\partial x_i}\left[\overline{\lambda\frac{\partial T}{\partial x_i}} - \overline{\rho}(\widetilde{u_i h_s} - \tilde{u}_i\tilde{h}_s)\right] \\ + \overline{\tau_{ij}\frac{\partial u_i}{\partial x_j}} - \frac{\partial}{\partial x_i}\left(\overline{\rho\sum_{k=1}^{N} V_{k,i}Y_k h_{s,k}}\right) + \overline{\dot{\omega}}_T\end{aligned} \tag{2.40}$$

where:

$$\overline{\frac{Dp}{Dt}} = \frac{\partial \overline{p}}{\partial t} + \overline{u_i\frac{\partial p}{\partial x_i}} \tag{2.41}$$

and the unresolved quantities are[36]:

- Reynolds stresses ($\widetilde{u_i u_j} - \tilde{u}_i\tilde{u}_j$), which require SGS models,
- unresolved species fluxes ($\widetilde{u_i Y_k} - \tilde{u}_i\tilde{Y}_k$) and enthalpy fluxes ($\widetilde{u_i h_s} - \tilde{u}_i\tilde{h}_s$),
- laminar diffusion fluxes,
- averaged reaction rate, $\overline{\dot{\omega}}_k$,
- the averaged product between pressure and velocity, $\overline{u_i(\partial p/\partial x_i)}$.

Unlike DNS, underlying information over unresolved small scales vanishes[30], however, in comparison with Reynolds ensemble averaging, LES gives instantaneous resolved fields[36].

Post filtering, the filtered Navier-Stokes equation are hereby[30]:

$$\frac{\partial \tilde{u}_i}{\partial t} + \frac{\partial \tilde{u}_i\tilde{u}_j}{\partial x_j} = -\frac{1}{\rho_0}\frac{\partial \tilde{p}}{\partial x_i} + \frac{\partial}{\partial x_j}\nu\left(\frac{\partial \tilde{u}_i}{\partial x_j} + \frac{\partial \tilde{u}_j}{\partial x_i}\right) + \frac{1}{\rho_0}\frac{\partial \tau_{SGS}}{\partial x_j} \tag{2.42}$$

To account for the unresolved scales that are smaller than the filter length, the sub-grid stress, τ_{SGS}, is introduced. This parameter expresses the flux of momentum from the large scales onto the unresolved ones, granted it remains as a closure problem itself, even if for just the microstructure[7]:

$$\tau_{SGS} = -\rho_0\left(\widetilde{u_i u_j} - \tilde{u}_i\tilde{u}_j\right) \tag{2.43}$$

One of the first sub-grid scale (SGS) models is the Smagorinsky model[44]. It is based around on the assumption of the eddy viscosity (ν_t) to model the sub-grid stress[7]:

$$\tau_{SGS} = \nu_t\left(\frac{\partial \tilde{u}_i}{\partial x_j} + \frac{\partial \tilde{u}_j}{\partial x_i}\right) \tag{2.44}$$

Moreover over this may be found in Ferziger et al.[8].

In recent years, improved models have came to life. For instance, within STAR-CCM+, a more sophisticated model for CFD is available[7, 43]: the Wall-Adapting Local Eddy-viscosity (WALE)[43], which has the possibility to incorporate all the relevant turbulence

structures for the energy dissipation (while considering the usage of both the local strain and rotation rates), as well as the fact that it uses only local information[36]. In addition, it enables the reduction of eddy-viscosity to zero at the wall without any sort of help from damping functions[29].

2.4 Chemistry for turbulent combustion

2.4.1 Introduction

As mentioned, recreating flames implies accounting for several hundreds of species and, thereby, thousands of reactions[36, 37]. The current option lies on the implementation of detailed mechanisms, which contain a considerable amount of reactions (in comparison with the theoretical systems describing real flames), however, such mechanisms still remain quite costly[37]. A more appealing solution passes by utilizing global (or reduced) mechanisms, i.e., simplified chemical schemes that contain only the predominant chemical equations that determine the chemical scheme, thus reducing in a significant way the amount of time necessary to conduct CFD[37].

Consequently, it is important to explain why building this models is, to this day, quite difficult[36]:

- each admitted species requires additional balance equations[36],
- complex terms such as transport coefficients and chemical reaction rates must be accounted and they increase the computational time[43],
- connecting turbulence scales with chemical scales[36].

Many different approaches have been proposed to decrease chemical schemes, all of which based around the principal that the fastest chemical time scales can be neglected[36].

2.4.2 Reduced chemical models

The development of global schemes from complex chemical schemes relies on two major assumptions[36]:

- quasi-steady approximation: in order to reach equilibrium state, only a few intermediate species/radicals are admitted.
- partial chemical equilibrium: it is assumed that some elementary reactions of the chemical have reached equilibrium[36].

A suggested example would be that of Smoke[45] and Peters[33, 34]:

$$\begin{aligned} &(I) \quad CH_4 + 2H + H_2O = CO + 4H_2 \\ &(II) \quad CO + H_2O = CO_2 + H_2 \\ &(III) \quad H + H + M = H_2 + M \\ &(IV) \quad O_2 + 3H_2 = 2H + 2H_2O \end{aligned} \tag{2.45}$$

with the corresponding reaction rate terms:

$$\begin{aligned} \dot{\omega}_I &= k_{11} \left[CH_4\right] \left[H\right] \\ \dot{\omega}_{II} &= \frac{k_{9f}}{K_3} \frac{\left[H\right]}{\left[H_2\right]} \left(\left[CO\right] \left[H_2O\right] - \frac{1}{K_{II}} \left[CO\right] \left[H_2\right] \right) \\ \dot{\omega}_{III} &= k_5 \left[H\right] \left[O_2\right] \left[M\right] \\ \dot{\omega}_{IV} &= k_{1f} \frac{\left[H\right]}{\left[H_2\right]^3} \left(\left[O_2\right] \left[H_2\right]^3 - \frac{1}{K_{IV}} \left[H\right]^2 \left[H_2O\right]^2 \right) \end{aligned} \tag{2.46}$$

The constant reaction rates are given by[36]:

$$\begin{aligned} &(1\text{f}) \quad H + O_2 \rightarrow OH + O \\ &(5) \quad H + O_2 + M \rightarrow HO_2 + M \\ &(9\text{f}) \quad CO + OH \rightarrow CO_2 + H \\ &(11) \quad CH_4 + H \rightarrow CH_3 + H_2 \end{aligned} \tag{2.47}$$

The aforementioned assumptions give rise to new difficulties since it is not easy to identify the limiting steps, in-equilibrium reactions and quasi-steady state species[37], as the matching reaction rate expressions still carry often stiffer mathematical formulations[36].

2.4.3 Chemistry closure models

As previously discussed in Sec. §2.4.2, there is also a need for a closure model regarding the combustion process.

Currently, two different approaches have been established to tackle the main parameter regarding chemical effects: heat release[7]. On one hand, one may solve both the transport and reaction of the several admitted species throughout the computational domain. This technique can be useful when kinetic phenomena, such as flame ignition, flame quenching, slow pollutants formation or extinction have to be considered[43]. On the other hand, one may also use already computed data, in the form of a table, to correlate important combustion parameters to a single reaction scalar[11].

Depending on the type of software used for CFD, there could be several different combustion closure models available, thereby, the following sections will be discussed in the context of the chosen program to compute the simulations, that is, STAR-CCM+, whose permission to use was given by Siemens Digital Industries Software, in Leuven[43].

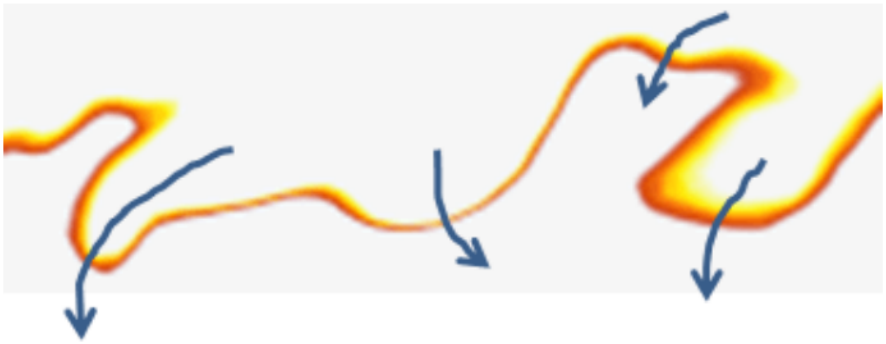


Figure 2.7: Illustration of a flamelet[43].

Flamelet

A possible definition for flamelet refers to a turbulent premixed flame regime wherein no flame quenching is occurring[36].

Flamelet models avoid the computational expense of complex chemistry calculations by preemptively calculating the chemistry in gas-phase laminar flames, using either 0D or 1D geometries with detailed chemical mechanisms[43]. A reduced set of variables are used to parameterize and tabulate the species from these simple flames, which subsequently, are interpolated in the 3D simulation of turbulent flames[7].

In the following illustration, Fig. 2.7, the dark region reveals a thin reaction front wherein reactions happen faster than turbulent mixing. As for the intermediate species: they do not exist for long enough to be transported out of the turbulent mixing[43].

Within STAR-CCM+, all flamelet models use mixture fraction[ii] as one parameter. Since atomic elements are conserved in chemical reactions, the mixture fraction becomes therefore conserved, ergo, the corresponding transport equation shall not contain a source term[43].

Some variables such as mixture fraction, reaction progress, scalar dissipation and enthalpy describe the thermochemical state (species composition and temperature) of the system[36]. Due to the fact that the number of parameters is small, it is feasible to use Presumed Probability Density Functions (PPDF[iii]) in order to account for fluctuations. The flamelet models use both beta PPDF functions for mixture functions and delta functions for other variables like enthalpy and scalar dissipation[43].

Flamelet models are commonly applied in (multi) gas-phase flames where the thermochemistry appears nearby the flamelet manifolds[36]. Within the available flamelet models in STAR-CCM+, a detailed look will be given to Flamelet Generated Manifold model (FGM).

[ii] Atomic mass fraction resulting from the fuel stream[43].

[iii] PPDF serve as a PDF with fixed shape, parameterized with a few amount of variables, a suggestion proposed by Williams[52].

FGM

The method of tabulated chemistry is based on generating look-up tables through a reduced amount of complex chemistry before starting the simulation[7]. Notable quantities such $\dot{\omega}$ and Y are computed as functions of the progress variable Y and mixture fraction Z[43]. A widespread method that is built upon this concept is the Flamelet Generated Manifold (FGM), a model based on low-dimensional representations of chemically reacting flow situations[40, 48], i.e., that has minimal computational cost and takes into consideration detailed chemistry[43].

The FGM method consists mainly of three steps[43]: first, it generates representative flamelets, then it stores said flamelets in a look-up table, and finally couples the table with the flow solver. In other words, FGM sets first one-dimensional laminar flame elements, so that afterwards three-dimensional flames can be built[7]. These flamelets can be computed by solving one dimensional flamelet equations grounded on the complex chemical schemes[49].

Thereafter, the data generated from the flamelets is accumulated in a n-dimensional manifold[43]. In the interest of this thesis, and for the sake of simplifying as much as possible the system, the used manifold only depends on two inputs: the progress variable ($\mathrm{Y} = \sum_{k=1}^{N} \alpha_i Y_i$), and the mixture fraction ($\mathrm{Z} = m_f/(m_f + m_{ox})$), which are later saved as a table wherein the solver may extract data[43]. Note that Y is the parameter that allows the solver to find the data, meaning it only determines the state of the flame according to this variable[7]. Fig. 2.8 showcases this concept through a screenshot taken in STAR-CCM+, while testing CFD[43]. Lastly, the coupling of the solver with the look-up table: during CFD, the solver resolves transport equations for the mixture fraction and progress variable[7].

The transport equation for progress variable, Y, is described as follows[43]:

$$\frac{\partial (\rho \mathrm{Y})}{\partial t} + \nabla (\rho \vec{u} \mathrm{Y}) - \nabla (\Gamma_{\mathrm{Y}} \nabla \mathrm{Y}) = \dot{\omega}_{\mathrm{Y}} \tag{2.48}$$

where the last term, $\dot{\omega}_{\mathrm{Y}}$, stands for the progress variable source term, which needs to be modeled in order to account for the chemistry-turbulence interaction, being the main influence for flame propagation[7]. The increase in temperature due to combustion is computed through species enthalpy and heat capacity.

Despite FGM being suitable for all (partially-)premixed flames wherein the flamelet assumption is valid (i.e., there are infinitely fast chemical reactions undergoing[36]), it is most suitable for gas turbine simulations, with constant pressure combustors, at full-load, or, for which statistically-steady turbulent combustion occur[43].

STAR-CCM+ offers the possibility to customize the used reactor type: if FGM is selected, the software calculates the chemical effects using detailed chemical mechanisms in simple 0D or 1D laminar flamelet geometries[43]. The results are afterwards tabulated and interpolated in a 3D simulation of a turbulent flame[43]. On a side note, in case TFM[iv]

[iv]The Thickened Flame Model (TFM) is a model that artificially thickens premixed flame fronts in order to resolve them on the mesh, by increasing thermal and species diffusivities[43].

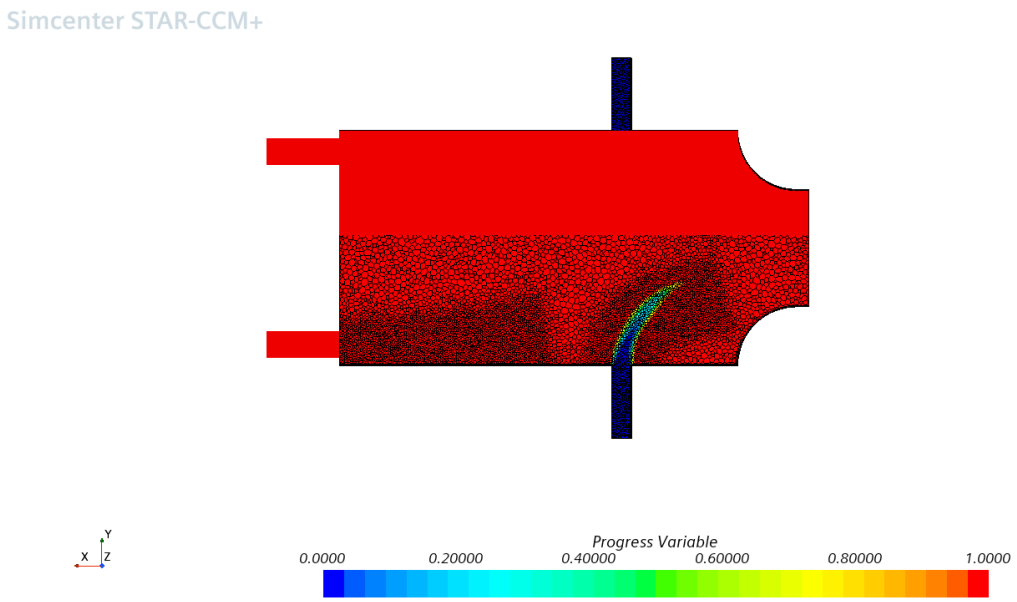


Figure 2.8: Cross-section of progress variable profile (reduced temperature in this case) for STAR-CCM+. The variable ranges from 0 (fresh gas) and 1.0 (burnt gas).

is selected within FGM, the obtained progress variable will be the defining parameter to compute the thickness of the flame.

Several models exist, whose purpose is to compute $\dot{\omega}_Y$ (TFC, Kinetic Rate, Coherent Flame Model et.al.)[7], however, mainly Turbulent Flame Speed Closure was explored. A good review of the restrictions of these configurations might be found in Kee et.al.[16].

Transport of reacting species

In terms of transport equations, STAR-CCM+ solves the mass fraction for all the involved species in the chemical reactions[43]. Such species mass fractions are then passed to a separate chemistry solver which returns the amount of product. Fig. 2.9 illustrates the process: the dark region depicts a thick reaction front[43]. Because some reactions are slower than the turbulent mixing, said phenomena causes some slowly-reacting intermediate species to escape said dark region so that they may proceed mixing further downstream[43].

Complex chemistry

The Complex Chemistry model carries a stiff solver to integrate the chemistry over a time-step via what is denoted as chemistry acceleration techniques, such as Dynamic Mechanism Reduction, In-Situ Adaptive Tabulation (ISAT[v]), and more importantly, Clustering, to

[v]Proposed by Pope[38] and Yang and Pope[53], model whose purpose is to efficiently extract information from chemical look-up tables.

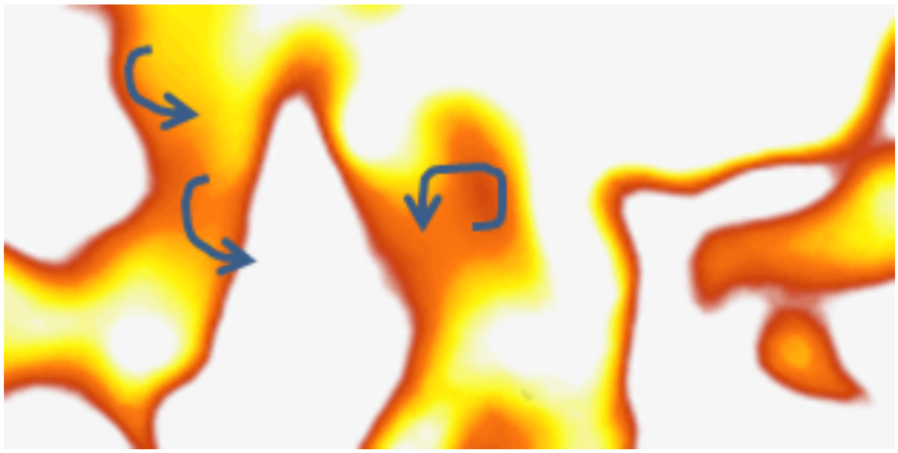


Figure 2.9: Illustration of reacting species transport[43].

mitigate this expense[43].

Thanks to Complex Chemistry, STAR-CCM+ is allowed to model kinetic phenomena such as flame ignition, slowly forming pollutants, flame quenching and extinction[43]. The methodology behind lies in simulating turbulence-chemistry interactions through its submodels (Laminar Flame Concept (LFC), Eddy Dissipation Concept (EDC[vi]) and, also in this case, TFC). Regarding its accessibility, Complex Chemistry models are typically imported in CHEMKIN format.

2.4.4 Turbulence-chemistry closure models: TFC

TFC serves as a model that propagates the flame front at specified flame speeds[43]. Upon modeling the system, this mechanism was chosen because it allows calibrating the flame length to a certain length via a scaling factor, comparable to that of experimental data[7]. Eq. (2.49) represents the computation of the progress variable source term while using TFC[43]:

$$\dot{\omega}_{\mathrm{Y}} = A\rho_u\nu_T\left|\nabla \mathrm{Y}\right| \tag{2.49}$$

where A is the scaling factor, ν_T is the turbulent flame speed and ρ_u is the density of the unburnt mixture[7].

Obtained from Gülder's correlation[13], the turbulent flame speed can be approximated by the model of Zimont[54], which bases itself on the laminar flame speed when turbulent variables increase the burning speed. Such relation with the flame speed is shown in Eq. (2.50) and it contains the stretch factor, G, which is the parameter that takes the effect of flame front stretch into account, the velocity fluctuations u', the laminar burning velocity

[vi]Devised by Magnussen and Mjertager[35], this model directly extends the Eddy Break-Up (EBU) model to non-premixed combustion[36].

ν_L, the unburnt thermal diffusivity α_u and lastly the turbulent length scale I_l[7]:

$$\nu_T = \frac{1}{2} G \left(u'\right)^{3/4} \nu_L^{1/2} \alpha_u^{-(1/4)} I_l^{1/4} \tag{2.50}$$

3 Burner configuration

3.1 Introduction

Within the scope of this thesis, a small scale burner inspired by the real life HBK-S FLOX Burner model (by Siemens[43]), is used to analyse the applicability of reduced mechanisms through a numerical study on flame structure, primarily focusing on parameters such as mean chemistry heat release and flame shape. Said combustor was modeled and underwent testing by means of the software STAR-CCM+.

The present chapter aims to briefly cover the following aspects:

- overview of the combustor layout,
- operating conditions for the conducted CFD simulations,
- brief discussion on specific inner model parameters.

3.2 Geometry

The used model for this work is adapted from a small scale burner used by the German Aerospace Center[7] (DLR), which performs experiments on industrial level turbulent combustion flows[42]. A side view of the complete setup is projected in Fig. 3.1. Preheated air (e.g. exhaust gases) passes by the distribution ducts (1) into the hexagonal shaped combustion chamber (2). Simultaneously, the air-fuel premix is injected via the inlet ducts (3). Afterwards, the resulting products from the reaction enter the converging-diverging nozzle (4), which directs the flow to the outlet. Moreover, Fig. 3.2 provides with an auxiliary perspective of the combustion chamber, containing its front view as well as some additional relevant dimensions. The main added elements were the twelve side inlet ducts from which fuel gets injected. The distribution ducts serve only to recreate a more realistic flow profile inside the combustion chamber.

3.3 Operating conditions

The main operating conditions can be divided into operating points[7]. The first operating point is referred to as Case I (see §3.5), where fuel consists exclusively of natural gas, is

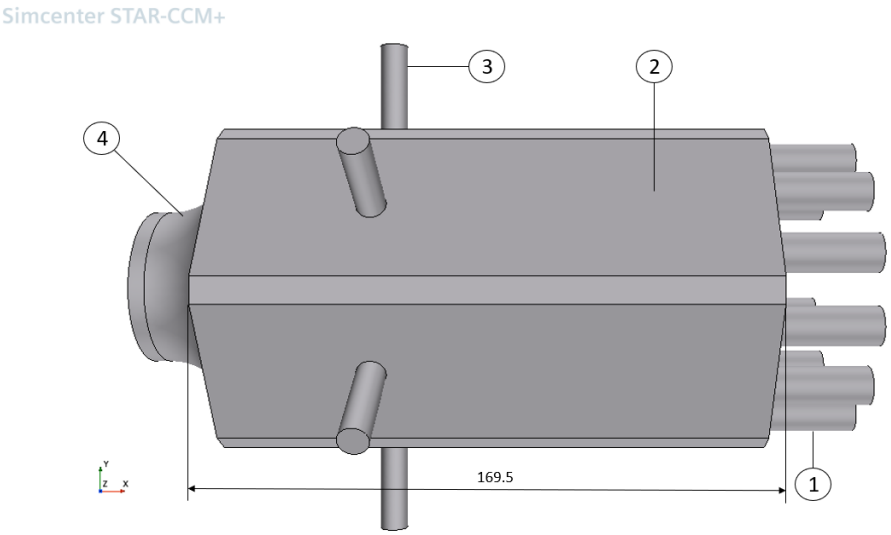


Figure 3.1: Side view of the geometry used in numerical study with flow moving from right to left: 1) Exhaust distribution duct; 2) Combustion chamber; 3) Premixing duct; 4) Entrance to converging-diverging nozzle.

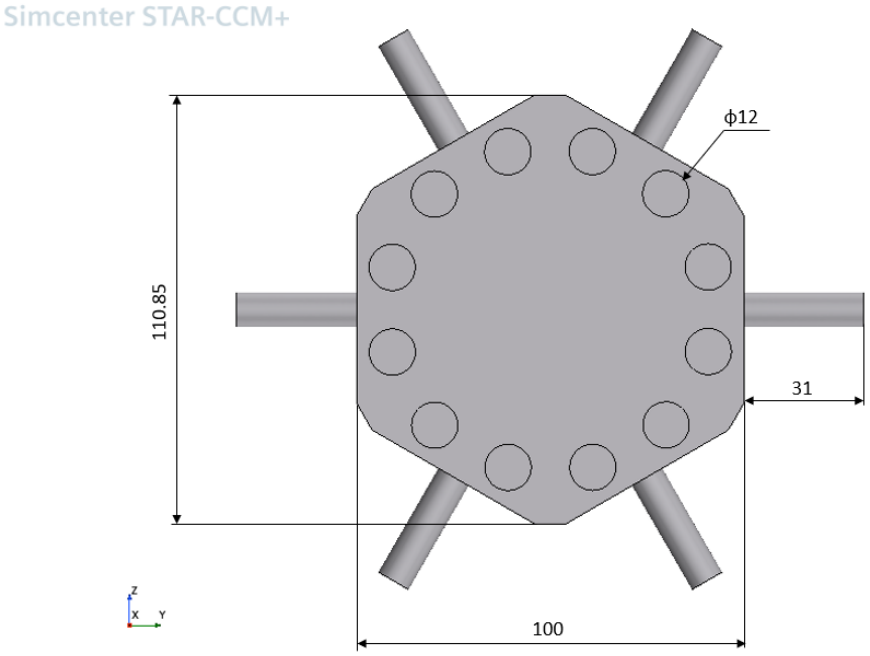


Figure 3.2: Front view of the combustion chamber.

introduced. The remaining cases fall on the second operating point, wherein a fuel premixture of methane with 60% hydrogen was considered. Properties for both operating points can be found in Table 3.1.

Table 3.1: Operating conditions for all tested cases[28].

Operating Conditions	p [bar]	u [m/s]	T_{air} [K]	$\dot{m}_{air}$ [g/s]	$\dot{m}_{CH_4}$ [g/s]	λ [-]	$\dot{m}_{H_2}$ [g/s]	$[H_2]$ [%]	T_{ad} [K]	c [m/s]
I	8	110	723.15	574	21.87	1.54	0	0	2016	901
II	8	110	723.15	574	13.61	1.82	2.44	60	1900	874

As observed, both operating settings do not differ much. Properties such as pressure, velocity inside the premixing ducts, preheating temperature or air mass flow are all alike[7]. Both operating points average a total mass flow of 590 g/s at the outlet, with the first point indicating an equivalence ratio of 65% while the second one shows 55%. The core difference lies on the addition of hydrogen to the fuel and the increase of air-fuel equivalence ratio, λ, which causes the flames to become leaner as well as a subsequent addition of thermal power to the system[7].

3.4 Numerical details

Meshing is a relevant topic regarding CFD, so, the present section will give some numerical details on that matter, as well as on other needed aspects.

Mesh

The mesh discussed in this section is used for both the RANS and LES studies[7]. A polyhedral mesh model was selected as the volume mesh because it produces a more accurate solution, whilst remaining a relatively efficient and accessible body to built[43]. Across the domain, different refinement regions are introduced in order to achieve the necessary cell sizes to sufficiently solve the physics, while keeping cell count to a desirable minimum.

The combustor cross-section plane is depicted in Fig. 3.3. Some refinement regions are referenced by numbers, namely the combustion chamber (1), the flame region (2), the premixing duct (3) and the exhaust gases distribution duct (4).

Furthermore, Fig. 3.4 projects a cross-section taken screenshot of the STAR-CCM+'s field function: LES delta, which gives information about each cell's filter size[43] and therefore provides an overview of relevant mesh data contained in Table 3.2.

Convective and Acoustic Courant number

Proceeding with the courant number (Co) and a variant thereof, the acoustic courant number (CFL). Both depend on the mesh size and time-step of the LES solver[7], however, while the Co number is based on the convective velocity, the Courant-Friedrichs-Lewy (CFL) number considers the summation of the convective velocity with the speed of sound[7]. A LES needs to attain a courant number close to unity to safeguard spatial and temporal

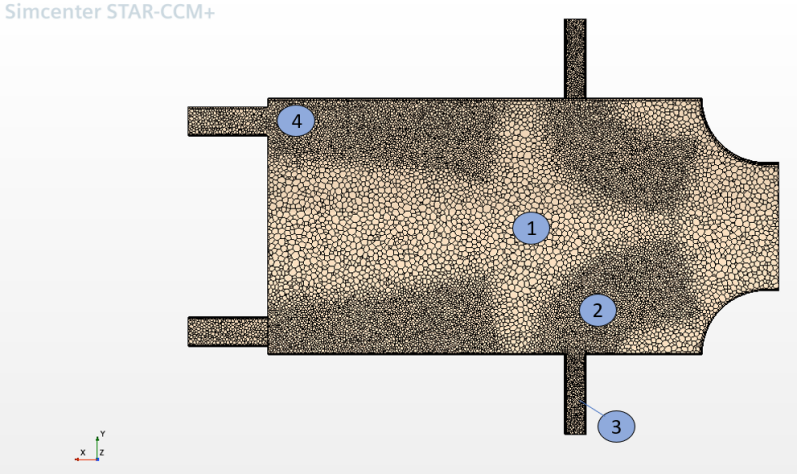


Figure 3.3: Cross-section view of the CFD mesh: 1) Combustion chamber; 2) Flame region; 3) Premixing duct; 4) Exhaust gas distribution duct.

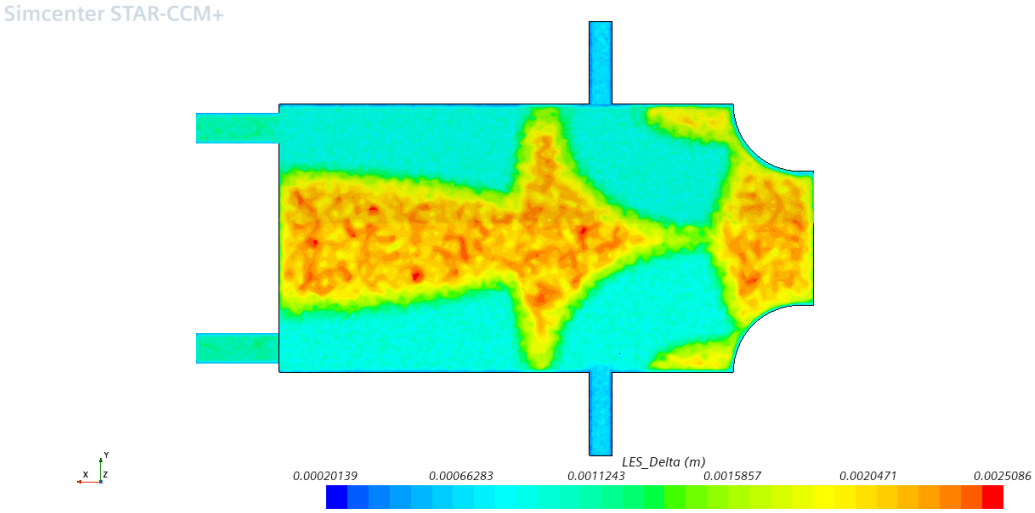


Figure 3.4: Cross-section view of the cell length across the burner.

fidelity[43], although that correlates into a drastic increase in computational cost. Fig 3.5 gives a quick overview of the obtained CFL profile of the burner.

Nevertheless, the CFL number shows an influence concerning the dissipation of acoustic waves[7], hence, to guarantee stable acoustic effects with an optimal amount of computational cost, it is advised to set the acoustic CFL number a value, at least, equal to or lower than 0.7, while the convective CFL number should be slightly lower[20]. Furthermore, Eq. (3.1) describes the mathematical expressions for both dimensionless numbers[7]:

$$Co = \frac{|u|\,\Delta t}{\Delta x} \quad ; \quad CFL = \frac{(|u| + c)\,\Delta t}{\Delta x} \tag{3.1}$$

Values of the mesh CFL numbers can be found in Table 3.3.

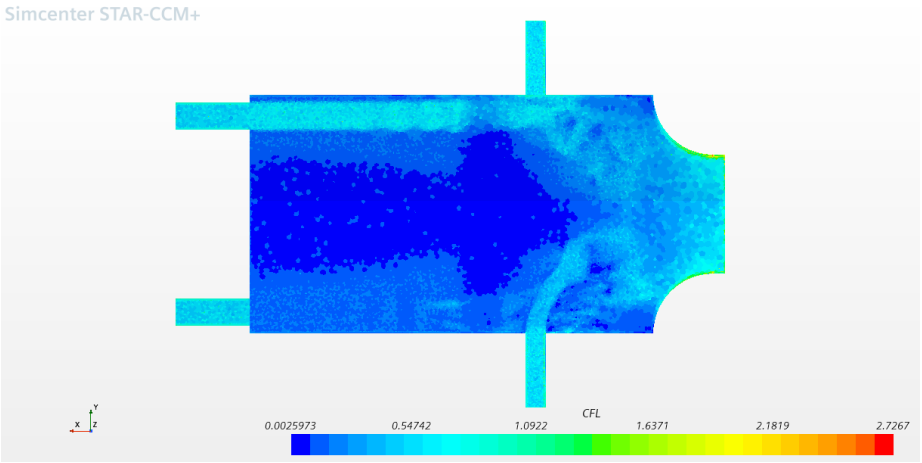


Figure 3.5: Cross-section view of the CFL number across the burner.

3.5 Model description

A quick overview of the adopted CFD settings for each case can be found in the present section.

Case I

The first case refers to operating condition I (see Table 3.1), with no hydrogen present in the fuel and a TFC rate coefficient, A, set to 2.0.

Case II

Second case (and onwards) refers both for operating condition II (see Table 3.1), the addition of hydrogen to the fuel and a TFC rate coefficient, A, set to 3.6.

Table 3.2: Details on used CFD mesh.

	Value	Unit
Number of cells	1,775,013	[-]
Cell size combustion chamber	~ 2.5	mm
Cell size flame region	~ 0.89	mm
Cell size premixing duct (coarse part)	~ 0.66	mm
Number of prism layers	3	[-]

Table 3.3: CFL numbers for relevant regions.

Region	Value
Combustion chamber	< 0.0026
Flame region	~ 0.7
Premixing ducts	~ 1

Table 3.4: CFD settings for case I.

RANS models		
Three-Dimensional	Flamelet Generated Manifold (FGM)	Segregated Flow
Steady	Turbulent Flame Speed Closure (TFC)	Segregated Fluid Enthalpy
Ideal Gas	Multi-Component Gas	K-Epsilon Turbulence
Reacting	Turbulent	Wall Distance
Gradients	Compressible	Two-Layer All y^+ Wall Treatment

Table 3.5: CFD settings for case II.

RANS models		
Three Dimensional	Flamelet Generated Manifold (FGM)	Segregated Flow
Implicit Unsteady	Turbulent Flame Speed Closure (TFC)	Segregated Fluid Enthalpy
Ideal Gas	Multi-Component Gas	K-Epsilon Turbulence
Reacting	Turbulent	Wall Distance
Gradients	Compressible	Two-Layer All y^+ Wall Treatment

Case III

Table 3.6 indicates the CFD settings for case III. Its notable change, in comparison to case II, is the shift of used solver, i.e., the switch from RANS code to LES code.

Table 3.6: CFD settings for case III.

LES models		
Three Dimensional	Flamelet Generated Manifold (FGM)	Segregated Flow
Implicit Unsteady	Turbulent Flame Speed Closure (TFC)	Segregated Fluid Enthalpy
Ideal Gas	Multi-Component Gas	WALE Subgrid Scale
Reacting	Turbulent	Wall Distance
Gradients	Compressible	All y^+ Wall Treatment

Case IV and V

Due to the fact that the only objective difference between cases IV and V is the type of mechanism implemented (detailed mechanism for case IV and a reduced mechanism for case V), a single table, Table 3.7, is sufficient to indicate both cases CFD settings.

Table 3.7: CFD settings for case IV and V.

LES models		
Three Dimensional	Complex Chemistry	Segregated Flow
Implicit Unsteady	Turbulent Flame Speed Closure (TFC)	Segregated Fluid Enthalpy
Ideal Gas	Multi-Component Gas	WALE Subgrid Scale
Reacting Species Transport	Turbulent	Wall Distance
Gradients	Segregated Species	All y^+ Wall Treatment

3.6 Initializing solver

The present section elaborates on some intricacies that characterize the initialization of the solution, as well as to mention some chosen specific set values.

Convergence

The numerical quality of the CFD simulations can be evaluated in accordance to the level of convergence of the residuals[43] (e.g. continuity, momentum or energy), or other scalars of interest such as pressure or velocity. This is due to the fact that the error in the solution of a system of equations is quantified by the residual[7]. For each cell of the CFD domain, the degree to which discretized equations are fulfilled is quantified by its residual[43]. Henceforth, the goal is to acquire sufficiently converged small residuals, as well as convergence of scalars.

Physical time

Time-step was configured to 5 microseconds so, in order to reach sufficient convergence of the residuals and flow quantities[7], a total of 10 inner iterations per time-step were chosen. Lastly, all LES simulations were run at least a physical time of 0.02 seconds.

TFC set values

During RANS initialisation, different values for the rate coefficient of the turbulent flame speed closure, A, were chosen. For instance, $A = 3.6$ is chosen for all cases that contain hydrogen in the premix, while for the methane-only premixed flame, $A = 2.0$. The flame length is artificially tuned by adjusting this parameter[7, 43] (see Sec. §2.4.4).

Furthermore, some flames are rather more sensitive to a rate coefficient change than others[36]. Eq. (2.49) proves the flame length is also function of the turbulent burning velocity (and implicitly the laminar burning velocity). This means that flames, resulting from the combustion of lean premixed air-fuel containing hydrogen, are more prone to change their flame length[7], since the addition of hydrogen to such mixtures increases the laminar and turbulent burning velocity[27]. In other words, slightly changing the rate of coefficient A will have a bigger impact on a flame containing hydrogen, in comparison with a flame that does not.

Moreover, by artificially shortening the flames, the influence of compact flames on thermoacoustics could be explicitly studied[7]. Anyway, the flow field generated from the RANS is used to initialize the LES, as well as an acoustic suppression zone inside the outlet duct[7].

4 Results

4.1 Introduction

Now that the theory background has been provided and the settings of the used models have been described, one may finally start analysing the obtained results. In the interest of studying the potential of a reduced mechanism, one will hereby evaluate thermoinstabilities and flame structure[37], through the use of CFD, by comparing each case in accordance to some criteria such as the used turbulence and chemistry models, the utilized reaction mechanisms, and other notable quantities such heat release, percentile addition of H_2 to the fuel and flame shape, all while trying to answer the following questions:

1. in what way does Hydrogen influence the flame structure?

2. what is the main difference concerning the usage of FGM vs Complex Chemistry?

3. what are the notable differences observed between using the detailed and reduced mechanisms, respectively?

Because all cases share several common criteria, it is possible to provide beforehand, via Table 4.1, a quick overview of the major properties for each case. The following sections serve to directly compare cases on specific parameters with the goal of finding information to answer the aforementioned questions.

Table 4.1: Description of the major characteristics of each of the four analysed cases.

Case	Turbulence Model	Chemistry Model	Reaction Mechanism	Volume of H_2 in the fuel [%]
I	RANS	FGM	Detailed mech.	0
II	RANS	FGM	Detailed mech.	59.98
III	LES	FGM	Detailed mech.	59.98
IV	LES	Complex Chem.	Detailed mech.	59.72
V	LES	Complex Chem.	Reduced mech.	59.91

4.2 Addition of hydrogen to the premixed fuel

The main difference between cases I and II is the percentile addition of hydrogen to the premixed air-fuel: more precisely, the latter case contains a percentage volume of H_2 in the fuel, that constitutes around 60% its total fuel volume. This addition of H_2 is applied for cases II and onwards, as shown in Table 4.1. Figs. 4.1 and 4.2 give the mean chemistry heat release rate for cases I and II, respectively.

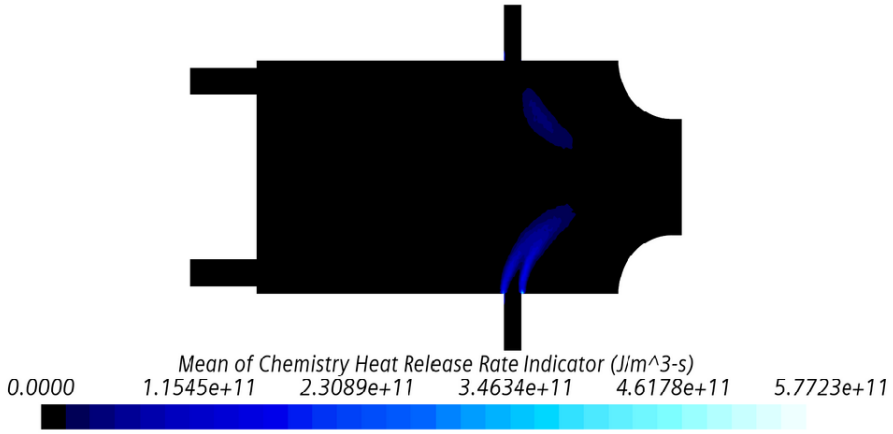


Figure 4.1: Mean of chemistry heat release rate for case I.

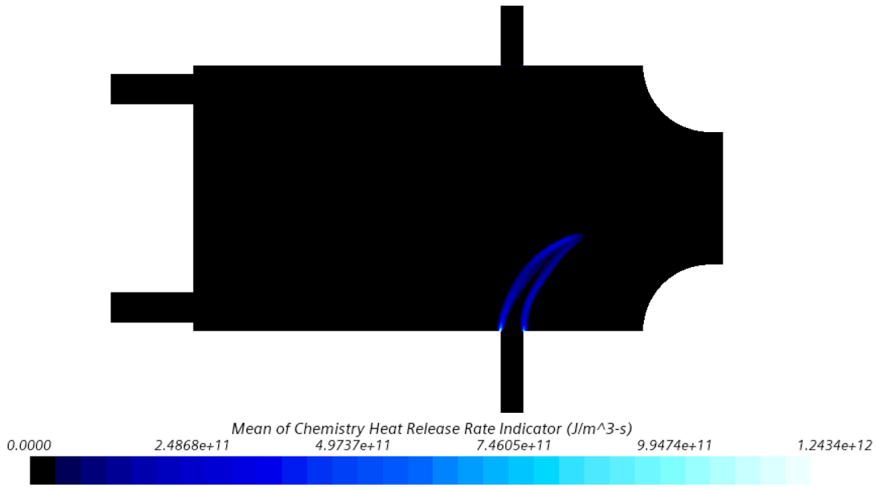


Figure 4.2: Mean of chemistry heat release rate for case II.

According to the displayed profiles, the addition of Hydrogen suggests a significant increase of the mean chemistry heat release rate, as well as an increase of the flame length. Said increase in flame length was unexpected, as studies performed by the DLR[42] state that adding hydrogen results in a shorter flame that leads to instabilities (since flame

length is directly connected to thermal instabilities near the wall[7]). The likely cause for such occurrence lies on the fact that the TFC rate coefficient, A, i.e., the scaling factor that calibrates the flame length and therefore artificially recreates the flame size with more or less accuracy, was set to 3.6 wherein flames of this sort which contain hydrogen (more sensitive than methane only flames, as explained in Sec. §3.6), should have had a larger set value (at least above 4). For case I, the rate coefficient rate, A, was set to a value of 2.0, which, for flames exclusively containing methane, is a reasonable guess.

4.3 RANS vs LES

As mentioned in Sec. §2.3.2, initializing the LES solver after establishing a flow field with RANS improves convergence and numerical stability, i.e., one can obtain a more accurate flame shape profile in which turbulence effects can be better visualized. As so, Figs. 4.3 and 4.4 compare the instantaneous temperature profile of cases II and III, in which the major difference is the used solver (purely RANS for case II and LES after RANS initialization for case III (which is done hereby for the remaining cases)).

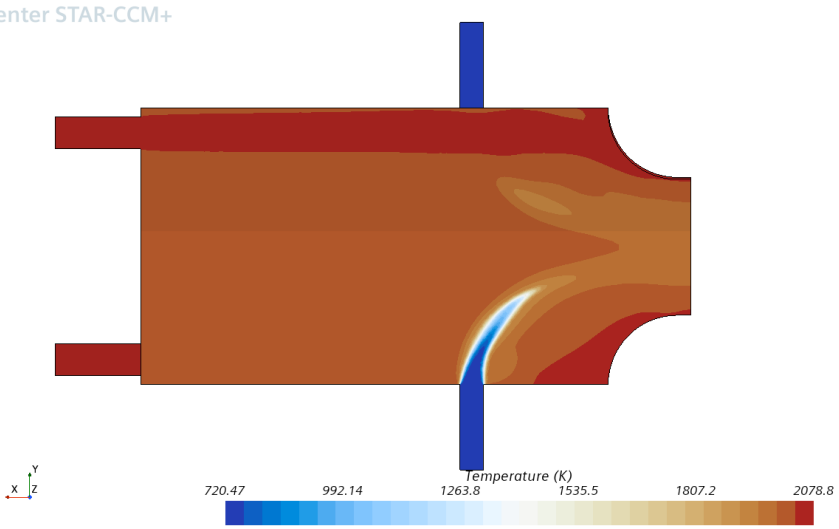


Figure 4.3: Instantaneous temperature profile of case II.

4.4 FGM vs Complex Chemistry

To put it simple, FGM bases itself on low-dimensional representations of chemically reacting flow situations resulting in minimal computational cost while accounting for detailed chemistry[36] (for further details check Sec. §2.4.3). On the other hand, Complex Chemistry carries a more powerful solver to integrate chemistry phenomena over a time-step, resulting in a more accurate depiction of turbulence-chemistry interaction, at the cost of

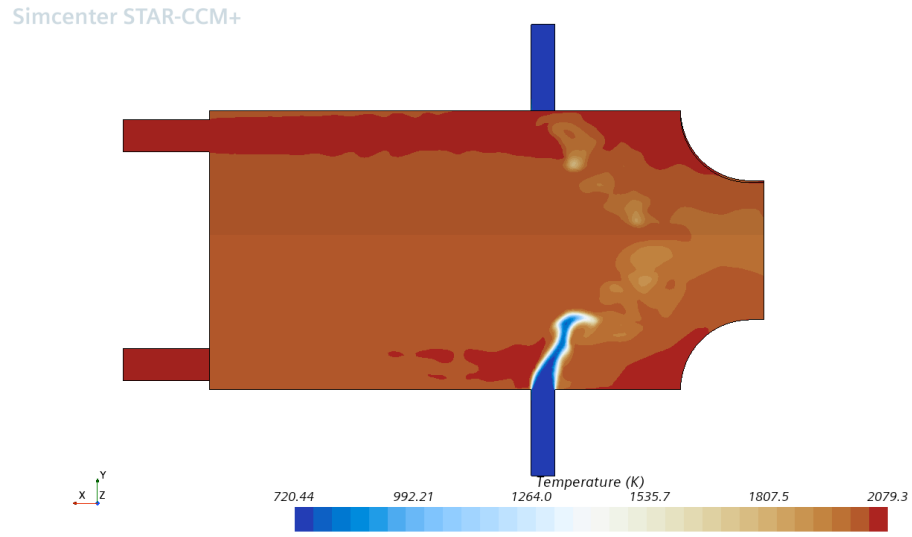


Figure 4.4: Instantaneous temperature profile of case III.

more computational resources[43]. Fig. 4.5 presents the temperature profile for case IV, whose main difference to case III was the selected chemistry model (Complex Chemistry).

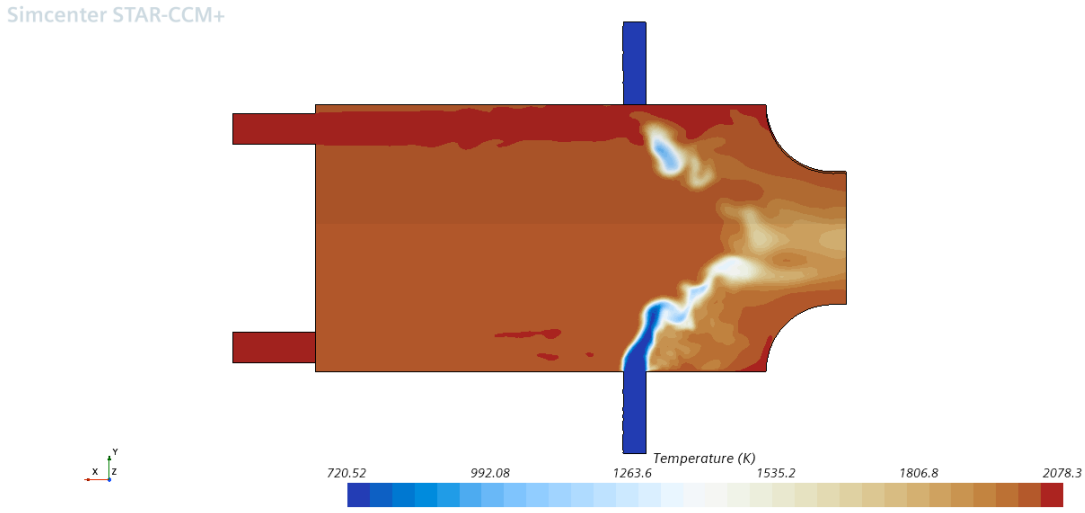


Figure 4.5: Instantaneous temperature profile of case IV.

As observed, the use of Complex Chemistry provides a more deformed shape of the flame, presumably because chemical effects such as heat release are accounted for further representation of the flame structure[36].

One may equally notice a significant amount of reactions occurring near the wall, which suggest an increase of thermoacoustic effects around that region for the present case[7]. This, however, is not the only sort of thermal-instabilities to occur: the wall-flame inter-

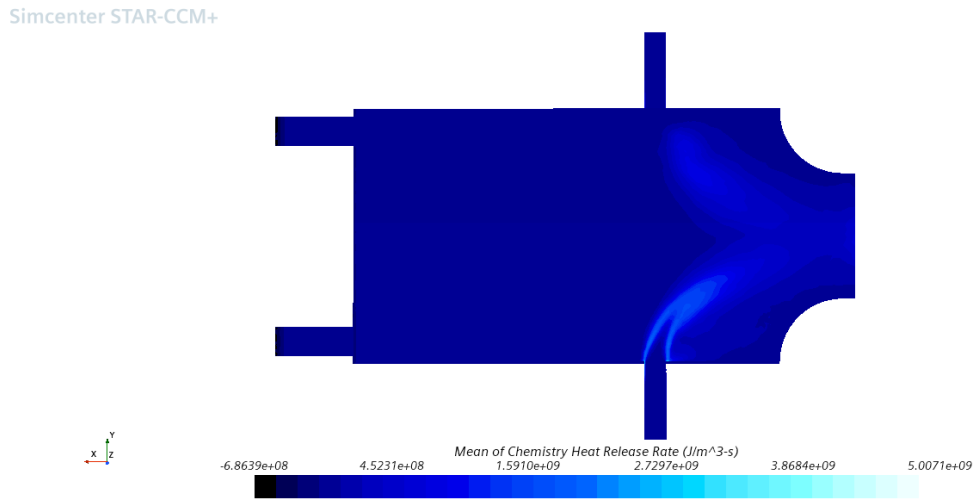


Figure 4.6: Mean of chemistry heat release rate for case IV.

actions, modeled thanks to the K-Epsilon submodel[i], also create flame quenching, which means there could be an enthalpy loss from the flow[36]. Fig 4.6 further asserts the enthalpy loss assumption. The wall presence also modifies turbulence scales therefore another model to represent this effect is needed: in this case the logarithmic laws model[15] was selected.

4.5 Detailed vs Reduced mechanisms

So far, all presented cases were generated through the use of the detailed mechanism. The final case resorts to the reduced one. Fig. 4.7 showcases the flame shape seen through the instantaneous temperature profile of a LES - Complex Chemistry simulation that uses the simplified chemical scheme. Polifke et.al.[37] suggests that some species become predominant in chemical schemes belonging to reduced mechanisms in order to validate the systems balance equations, which, in this case, would justify the flame size increase, since methane would likely be in available larger quantities.

Now, moving on to the mechanism analysis, the two main parameters which evaluate the performance of chemical package are its heat release and the geometrical center of the flame[7, 36, 37].

Fig. 4.8 showcases the mean of chemistry heat release rate profile from case V. As observed through the spectrum, the values for the chemistry heat release rate average are similar to case IV. This is a good indicator that both cases' geometric flame center is close, which means the reduced mechanism is showing it can "mimic" (with reasonable accuracy) the behaviour of a flame whose only difference is having a detailed mechanism (case IV).

Regarding the geometric center of flame, Table 4.2 provides the numerical relative coordinates of the geometric flame center for all cases. The volume report data represents

[i]Very well validated model for flows away from the wall[39].

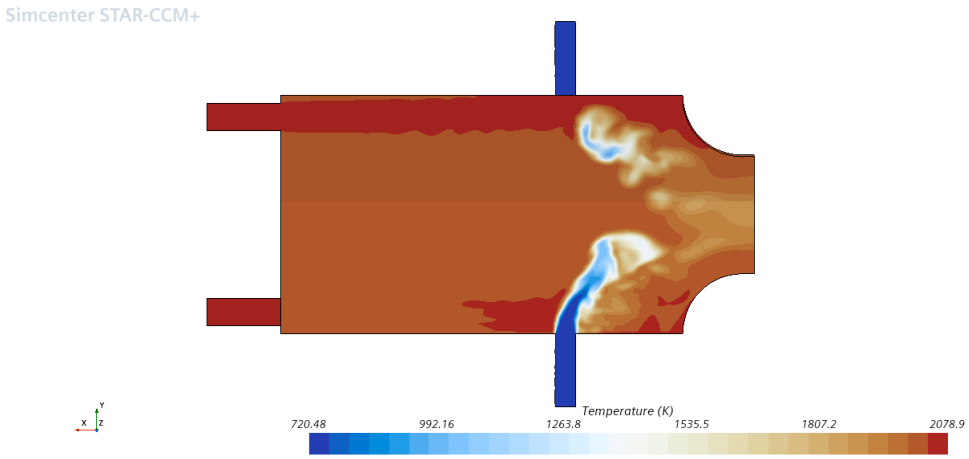


Figure 4.7: Instantaneous temperature profile of case V.

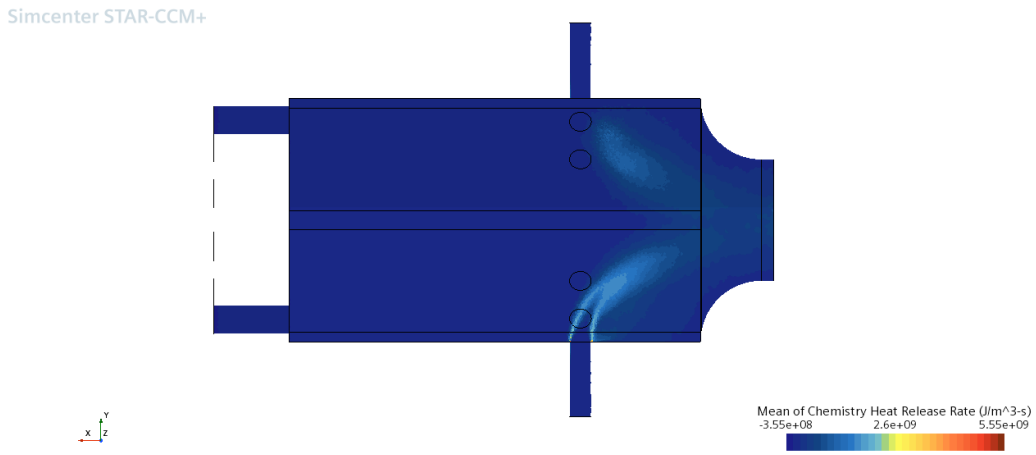


Figure 4.8: Mean of chemistry heat release rate profile for case V.

the relative coordinates of the geometric center flame of the flame.

For a better visualization of the data stored in Table 4.2, Figs. 4.9 to 4.13 contain the graphics providing the mean chemistry heat release rate for all spatial directions for all cases. The extracted data further indicates how consistent the behaviour of case V's flame (shape wise) is in comparison with the remaining examples. This not only shows the reduced mechanism works efficiently with LES and Complex Chemistry, but also with other relevant models such as RANS, TFC and FGM, as the obtained data seems converging.

It is also worth mentioning how the flame head from case V appears more "dense" as observed in case IV. This is likely due to the fact that the reduced mechanism encourages the abundance of methane[37] and therefore the flame appears to have a larger concentration of fuel at the top.

Table 4.2: Relative coordinates of the geometric center of flame for all DLR cases.

DLR case	Direction	vol. report 1	vol. report 2	vol. report 3	vol. report 4	vol. report 5	vol. report 6
I	X	0.4787	0.4795	0.4785	0.4775	0.4601	0.4784
	Y	0.0331	0.0161	−0.0162	−0.0312	−0.015	0.0155
	Z	0.0001	−0.0289	−0.0287	0	0.0265	0.0274
II	X	0.4806	0.4802	0.4803	0.4809	0.4805	0.4805
	Y	0.0355	0.0175	−0.0174	−0.0361	−0.0177	0.0176
	Z	0.0001	−0.0301	−0.0303	−0.0001	0.0305	0.0305
III	X	0.4775	0.4788	0.4784	0.4776	0.4781	0.4778
	Y	0.0341	0.0177	−0.0169	−0.0337	−0.0174	0.0171
	Z	−0.0001	−0.0298	−0.0292	0.0002	0.0292	0.0287
IV	X	0.4660	0.4660	0.4644	0.4632	0.4639	0.4644
	Y	0.0247	0.0135	−0.0137	−0.0249	−0.0132	0.0133
	Z	0.0004	−0.0236	−0.0226	−0.0004	0.0231	0.0215
V	X	0.4616	0.4624	0.4621	0.4606	0.4616	0.4601
	Y	0.0263	0.0136	−0.0134	−0.0261	−0.0136	0.0142
	Z	0	−0.0241	−0.0239	0.0002	0.0234	0.0241

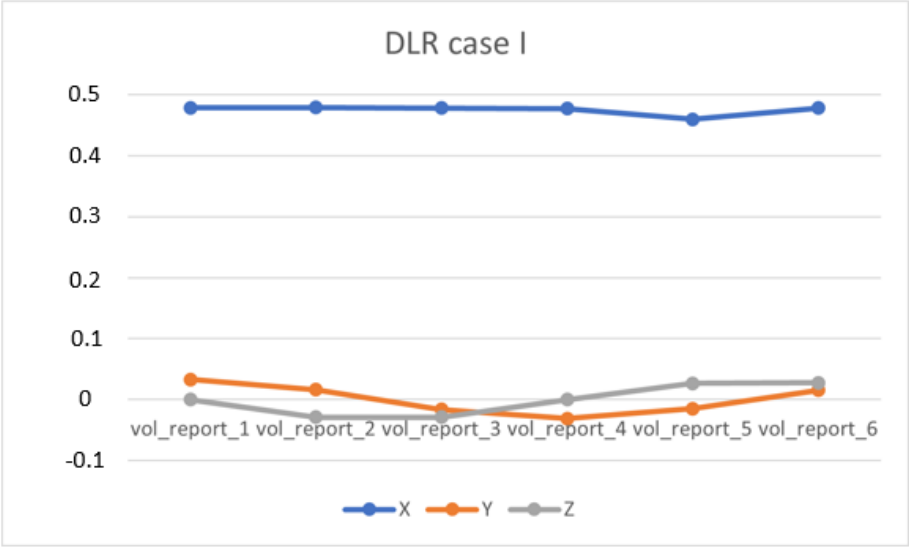


Figure 4.9: Evolution of the relative coordinates of the geometric center of flame for case I.

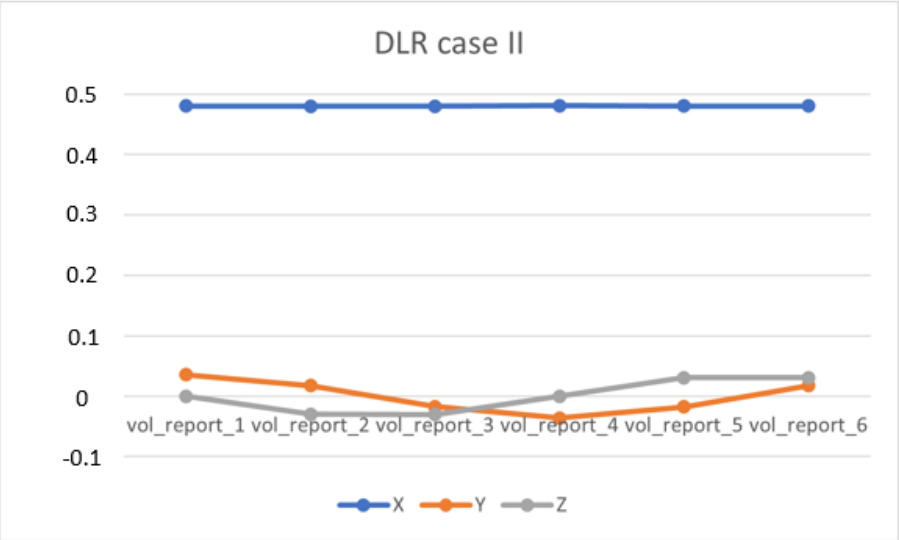


Figure 4.10: Evolution of the relative coordinates of the geometric center of flame for case II.

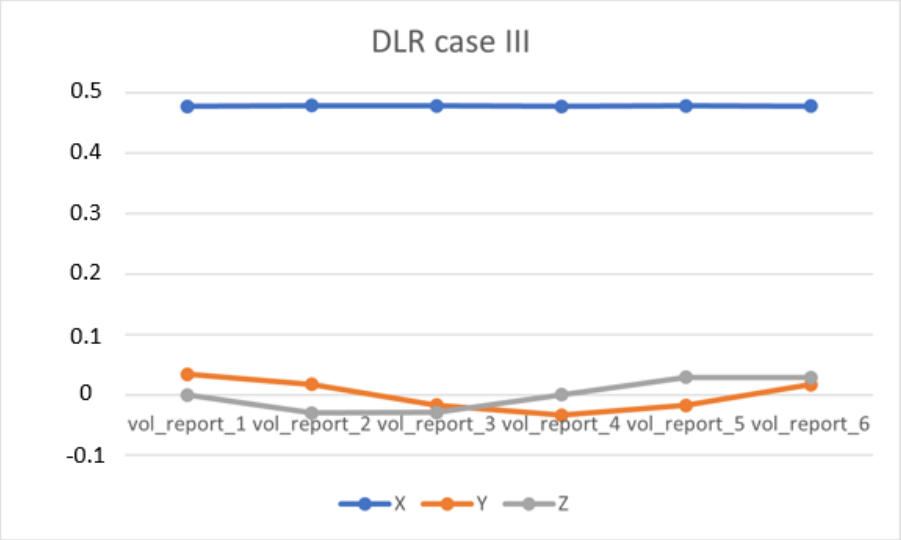


Figure 4.11: Evolution of the relative coordinates of the geometric center of flame for case III.

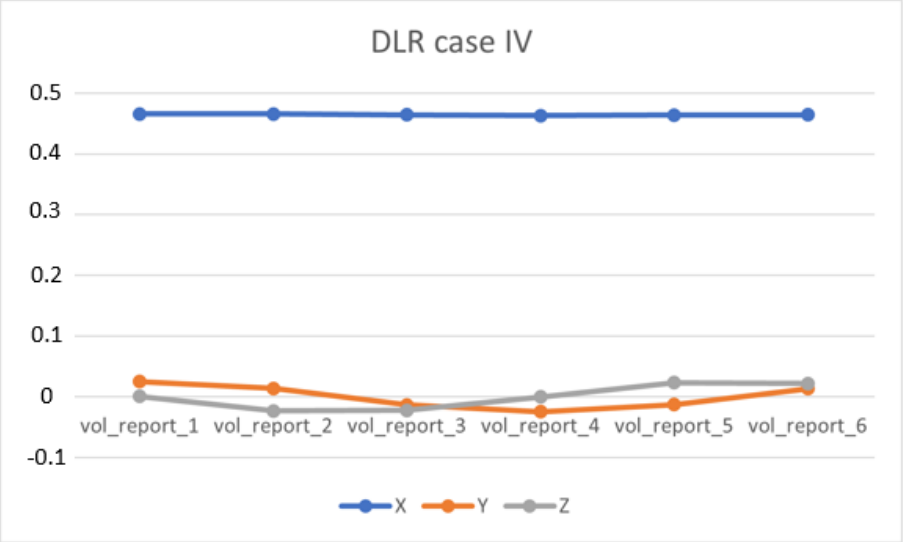


Figure 4.12: Evolution of the relative coordinates of the geometric center of flame for case IV.

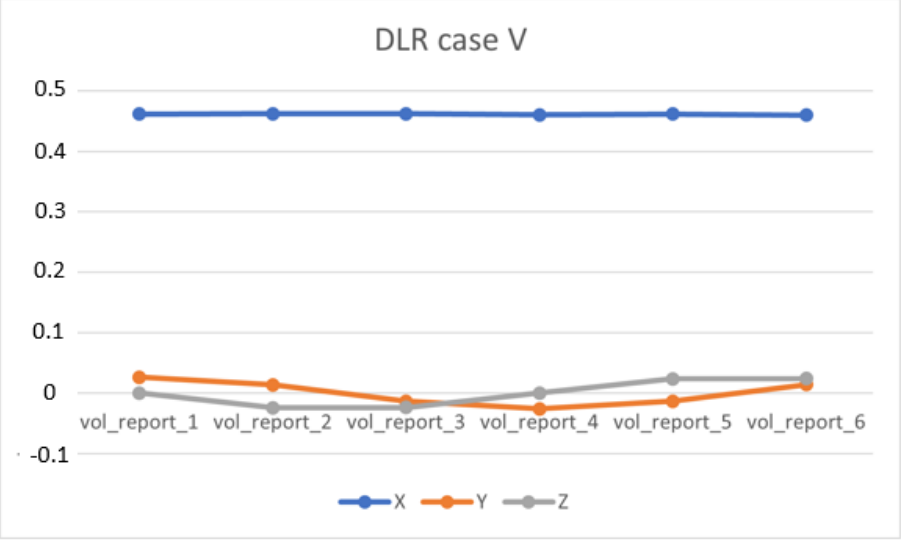


Figure 4.13: Evolution of the relative coordinates of the geometric center of flame for case V.

5 Conclusions

The burner configuration described in Chpt. §3 was used for an in-depth study of the flame structure. Several parameters, namely (mean) heat release and (instantaneous) temperature profiles were recorded in order to capture the flame shape response over the several utilized models and mechanisms. All the aforementioned properties were registered as the injected premixed fuel was burning inside the combustion chamber[7].

In case chemical effects resulting from the addition of hydrogen to the premix are modeled and thereby accounted, thermoinstabilities near the wall are thereby observed[6, 7], which may damage the burner overtime as well as promote thermoacoustic effects. Alongside the addition of hydrogen, the flame itself becomes more sensitive, which means, if the turbulence and chemistry models are not thoroughly modeled, the flame will not become as short as expected, as observed in case II.

In accordance to Sec. §2.4.3, even though chemistry closure models such as complex chemistry require more computation resources to simulate[36], as compared to FGM, they prove to be, indeed, worth using since the flame shape evidently changes in a significant way. Despite that, FGM serves as a good initial model to run before more complex cases are to be tested[43].

Lastly, the usage of a reduced mechanism did not change considerably the positioning of the geometric flame center, which, combined with the fact that the observed mean chemistry heat release rate evolution remained quite similar across all cases, leads to believe that the reduced mechanism may, indeed, serve as a viable tool to study flame combustion codes, in the sense that it adds up the additional advantage of demonstrating less computational cost to run[37], as explained in Sec. §2.4.2.

6 Future accomplishments

Overall, the work produced the expected results. Reduced mechanisms can see, indeed, a future in combustion of lean-premixed mixtures of air-hydrogen-methane in modern combustion systems.

Nevertheless, it is worth mentioning the unexpected result from case II. The fact that the flame did not shrink as much as expected leaves a desire to keep testing flame length in hydrogen-added lean premixed gases, even though there is already plenty of literature with diverse knowledge on the subject[6, 7, 36].

On another matter, thermoacoustic instabilities were a subject that ended up not being that much explored, simply because the obtained results were not looking as expected, meaning a lot more time would have been fairly needed in order to study it with due respect. With society moving on to greener energy sources, the combination of fuel with hydrogen (if not pure hydrogen mix) will eventually become a reality. Since hydrogen is commonly linked to flame shrinkage and, therefore, to thermoacoustic instabilities near the wall[7], it would make much sense to investigate more in that direction, in case the opportunity does come up.

Appendices

A Chapter 2

A.1 Averaging the balance equations: RANS

The following equation constitutes the averaged continuity equation[36, 38]:

$$\frac{\partial \overline{\rho}}{\partial t} + \frac{\partial}{\partial x_i}\left(\overline{\rho u_i}\right) = \frac{\partial \overline{\rho}}{\partial t} + \frac{\partial}{\partial x_i}\left(\overline{\rho}\overline{u_i} + \overline{\rho' u_i'}\right) = 0 \quad \text{or} \quad \frac{\partial \overline{\rho}}{\partial t} + \frac{\partial}{\partial x_i}\left(\overline{\rho}\overline{u_i}\right) = -\frac{\partial}{\partial x_i}\left(\overline{\rho' u_i'}\right) \tag{A.1}$$

where the following term, $\overline{\rho u_i}$, must be separately modeled.

Henceforth, applying this formalism to the conservation equations established in Sec. §2.1 results in[36]:

- Mass:

$$\frac{\partial \overline{\rho}}{\partial t} + \frac{\partial}{\partial x_i}\left(\overline{\rho}\tilde{u}_i\right) = 0 \tag{A.2}$$

- Momentum:

$$\frac{\partial \overline{\rho}\tilde{u}_i}{\partial t} + \frac{\partial}{\partial x_i}\left(\overline{\rho}\tilde{u}_i\tilde{u}_j\right) + \frac{\partial \overline{p}}{\partial x_j} = \frac{\partial}{\partial x_i}\left(\overline{\tau}_{ij} - \overline{\rho}\widetilde{u_i'' u_j''}\right) \tag{A.3}$$

- Chemical species:

$$\frac{\partial\left(\overline{\rho}\tilde{Y}_k\right)}{\partial t} + \frac{\partial}{\partial x_i}\left(\overline{\rho}\tilde{u}_i\tilde{Y}_k\right) = -\frac{\partial}{\partial x_i}\left(\overline{V_{k,i}Y_k} + \overline{\rho}\widetilde{u_i'' Y_k''}\right) + \overline{\dot{\omega}}_k \quad \text{for} \quad k = 1, N \tag{A.4}$$

- Enthalpy:

$$\begin{aligned}\frac{\partial \overline{\rho}\tilde{h}_s}{\partial t} + \frac{\partial}{\partial x_i}\left(\overline{\rho}\tilde{u}_i\tilde{h}_s\right) = \overline{\dot{\omega}}_T + \frac{\overline{Dp}}{Dt} + \frac{\partial}{\partial x_i}\left(\overline{\lambda\frac{\partial T}{\partial x_i}} - \overline{\rho u_i'' h_s''}\right) \\ + \overline{\tau_{ij}\frac{\partial u_i}{\partial x_j}} - \frac{\partial}{\partial x_i}\left(\overline{\rho\sum_{k=1}^{N} V_{k,i}Y_k h_{s,k}}\right)\end{aligned} \tag{A.5}$$

where:

$$\frac{\overline{Dp}}{Dt} = \frac{\partial \overline{p}}{\partial t} + \overline{u_i\frac{\partial p}{\partial x_i}} = \frac{\partial \overline{p}}{\partial t} +_i \frac{\partial \overline{p}}{\partial x_i} + \overline{u_i''\frac{\partial p}{\partial x_i}} \tag{A.6}$$

Bibliography

[1] KT Aung, MI Hassan, and GM Faeth. Effects of pressure and nitrogen dilution on flame/stretch interactions of laminar premixed h2/o2/n2 flames. *Combustion and flame*, 112(1-2):1–15, 1998.

[2] BF Boyarshinov, VI Titkov, and S Yu Fedorov. Momentum transfer in the boundary layer when there is acceleration and combustion of ethanol as it evaporates behind a barrier. *Combustion and flame*, 157(8):1496–1509, 2010.

[3] Henri BROCH. Mécanique des fluides. *Université de Nice Sophia Antipolis*, 2006.

[4] RS Cant and KNC Bray. Strained laminar flamelet calculations of premixed turbulent combustion in a closed vessel. In *Symposium (International) on Combustion*, volume 22, pages 791–799. Elsevier, 1989.

[5] Juan Pablo Castillo Alvarez et al. Simulación del flujo en torno a un vehículo tipo hatchback con modelos de turbulencia híbridos tipo ddes. 2022.

[6] Long-Qing Chen. Chemical potential and gibbs free energy. *Mrs Bulletin*, 44(7):520–523, 2019.

[7] Tim Dammers. Numerical study on the driving and damping of high-frequency instabilities in a jet flame combustor. pages 5–63, 2020.

[8] Joel H Ferziger and M Perić. Properties of numerical solution methods. *Computational methods for fluid dynamics*, 3(2):31–35, 2002.

[9] CG Fotache, H Wang, and Chung King Law. Ignition of ethane, propane, and butane in counterflow jets of cold fuel versus hot air under variable pressures. *Combustion and Flame*, 117(4):777–794, 1999.

[10] V Giovangigli and MD Smooke. Application of continuation methods to plane premixed laminar flames. *Combustion science and technology*, 87(1-6):241–256, 1993.

[11] Andrea Giusti and Epaminondas Mastorakos. Turbulent combustion modelling and experiments: Recent trends and developments. *Flow, Turbulence and Combustion*, 103(4):847–869, 2019.

[12] Irvin Glassman, Richard A Yetter, and Nick G Glumac. *Combustion*. Academic press, 2014.

[13] Ömer L Gülder. Turbulent premixed flame propagation models for different combustion regimes. In *Symposium (International) on Combustion*, volume 23, pages 743–750. Elsevier, 1991.

[14] S Kalamatianos, YK Park, and DG Vlachos. Two-parameter continuation algorithms for sensitivity analysis, parametric dependence, reduced mechanisms, and stability criteria of ignition and extinction. *Combustion and Flame*, 112(1-2):45–61, 1998.

[15] WM Kays and ME Crawford. Convective heat and mass transfer mcgraw-hill. *New York*, pages 255–282, 1993.

[16] Robert J Kee, Michael E Coltrin, Peter Glarborg, and Huayang Zhu. *Chemically reacting flow: theory, modeling, and simulation*. John Wiley & Sons, 2017.

[17] Essam E Khalil. Cfd history and applications. 2021.

[18] M Khosravy el_Hossaini. Review of the new combustion technologies in modern gas turbines. *Progress in Gas Turbine Performance*, pages 978–953, 2013.

[19] Andrei Nikolaevich Kolmogorov. The local structure of turbulence in incompressible viscous fluid for very large reynolds numbers. *Proceedings of the Royal Society of London. Series A: Mathematical and Physical Sciences*, 434(1890):9–13, 1991.

[20] Harmen Krediet. Prediction of limit cycle pressure oscillations in gas turbine combustion systems using the flame describing function. *University of Twente, Enschede*, 2012.

[21] Kenneth K Kuo. Principles of combustion. 1986.

[22] Davide Laera, Giovanni Campa, Sergio M Camporeale, Edoardo Bertolotto, Sergio Rizzo, Federico Bonzani, Antonio Ferrante, and Alessandro Saponaro. Modelling of thermoacoustic combustion instabilities phenomena: Application to an experimental test rig. *Energy Procedia*, 45:1392–1401, 2014.

[23] Mathias Lemke, Liming Cai, Julius Reiss, Heinz Pitsch, and Jörn Sesterhenn. Adjoint-based sensitivity analysis of quantities of interest of complex combustion models. *Combustion Theory and Modelling*, 23(1):180–196, 2019.

[24] B Lewis and G von Elbe. Combustion, flames and explosion of gases, iii-rd ed, 1987.

[25] Michael A Liberman. *Combustion Physics: Flames, Detonations, Explosions, Astrophysical Combustion and Inertial Confinement Fusion*. Springer Nature, 2021.

[26] Andrew Edward Lutz, Robert J Kee, and James Angus Miller. Senkin: A fortran program for predicting homogeneous gas phase chemical kinetics with sensitivity analysis. Technical report, Sandia National Labs., Livermore, CA (USA), 1988.

[27] C Mandilas, MP Ormsby, CGW Sheppard, and R Woolley. Effects of hydrogen addition on laminar and turbulent premixed methane and iso-octane–air flames. *Proceedings of the combustion institute*, 31(1):1443–1450, 2007.

[28] Payam Mohammadzadeh Keleshtery, Gerrit Heilmann, Christoph Hirsch, Lukasz Panek, Michael Huth, and Thomas Sattelmayer. High-frequency instability driving potential of premixed jet flames in a tubular combustor due to dynamic compression and deflection. In *Turbo Expo: Power for Land, Sea, and Air*, volume 84126, page V04AT04A060. American Society of Mechanical Engineers, 2020.

[29] Franck Nicoud and Frédéric Ducros. Subgrid-scale stress modelling based on the square of the velocity gradient tensor. *Flow, turbulence and Combustion*, 62(3):183–200, 1999.

[30] Frans TM Nieuwstadt, Jerry Westerweel, and Bendiks J Boersma. *Turbulence: introduction to theory and applications of turbulent flows*. Springer, 2016.

[31] Soham Pandya. Experimental study of proppant transport in horizontal and directional wells. 2016.

[32] Amar Patel, Song-Charng Kong, and Rolf D Reitz. Development and validation of a reduced reaction mechanism for hcci engine simulations. Technical report, SAE Technical Paper, 2004.

[33] N Peters. Numerical and asymptotic analysis of systematically reduced reaction schemes for hydrocarbon flames. In *Numerical simulation of combustion phenomena*, pages 90–109. Springer, 1985.

[34] Norbert Peters. *Turbulent combustion*. Cambridge university press, 2000.

[35] Michele Pisaroni, Rudi Sadi, and Domenico Lahaye. Counteracting ring formation in rotary kilns. *Journal of Mathematics in Industry*, 2(1):1–19, 2012.

[36] Thierry Poinsot and Denis Veynante. *Theoretical and numerical combustion*. RT Edwards, Inc., 2005.

[37] Wolfgang Polifke, Weiqun Geng, and Klaus Döbbeling. Optimization of rate coefficients for simplified reaction mechanisms with genetic algorithms. *Combustion and Flame*, 113(1-2):119–134, 1998.

[38] Stephen B Pope. Computationally efficient implementation of combustion chemistry using in situ adaptive tabulation. 1997.

[39] Stephen B Pope and Stephen B Pope. *Turbulent flows*. Cambridge university press, 2000.

[40] WJS Ramaekers, BA Albrecht, JA Van Oijen, LPH De Goey, and RGLM Eggels. The application of flamelet generated manifolds in modelling of turbulent partially-premixed flames. *RGLM Eggels*, 2005.

[41] L Selle. Simulation aux grandes échelles des couplages acoustique/combustion dans les turbines á gaz. *These de doctorat, INP Toulouse*, 2004.

[42] Junsu Shin and Hong-Gye Sung. Combustion characteristics of hydrogen and cracked kerosene in a dlr scramjet combustor using hybrid rans/les method. *Aerospace Science and Technology*, 80:433–444, 2018.

[43] Siemens Digital Industries Software. Simcenter star-ccm+ documentation: Version 2022.1.

[44] Joseph Smagorinsky. General circulation experiments with the primitive equations: I. the basic experiment. *Monthly weather review*, 91(3):99–164, 1963.

[45] Mitchell D Smooke. *Reduced kinetic mechanisms and asymptotic approximations for methane-air flames: a topical volume*. Springer, 1991.

[46] Gabriel Staffelbach, Jean Mathieu Senoner, Laurent Gicquel, and Thierry Poinsot. Large eddy simulation of combustion on massively parallel machines. In *International Conference on High Performance Computing for Computational Science*, pages 444–464. Springer, 2008.

[47] Adam M Steinberg, Peter E Hamlington, and Xinyu Zhao. Structure and dynamics of highly turbulent premixed combustion. *Progress in Energy and Combustion Science*, 85:100900, 2021.

[48] JA Van Oijen and LPH De Goey. Modelling of premixed laminar flames using flamelet-generated manifolds. *Combustion Science and Technology*, 161(1):113–137, 2000.

[49] JA Van Oijen, A Donini, RJM Bastiaans, JHM ten Thije Boonkkamp, and LPH De Goey. State-of-the-art in premixed combustion modeling using flamelet generated manifolds. *Progress in Energy and Combustion Science*, 57:30–74, 2016.

[50] D Veynante, J Piana, JM Duclos, and C Martel. Experimental analysis of flame surface density models for premixed turbulent combustion. In *Symposium (International) on Combustion*, volume 26, pages 413–420. Elsevier, 1996.

[51] D Veynante and T Poinsot. Reynolds averaged and large eddy simulation modeling for turbulent combustion. In *New tools in turbulence modelling*, pages 105–140. Springer, 1997.

[52] FA Williams. Turbulent combustion. In *The mathematics of combustion*, pages 97–131. SIAM, 1985.

[53] B Yang and SB Pope. Treating chemistry in combustion with detailed mechanisms—in situ adaptive tabulation in principal directions—premixed combustion. *Combustion and Flame*, 112(1-2):85–112, 1998.

[54] V Zimont, Wolfgang Polifke, Marco Bettelini, and Wolfgang Weisenstein. An efficient computational model for premixed turbulent combustion at high reynolds numbers based on a turbulent flame speed closure. 1998.

[55] Vladimir L Zimont. Gas premixed combustion at high turbulence. turbulent flame closure combustion model. *Experimental thermal and fluid science*, 21(1-3):179–186, 2000.